

Faster Adaptive Optimization via Expected Gradient Outer Product Reparameterization

Adela DePavia¹, Vasileios Charisopoulos², and Rebecca Willett^{1,2,3,4}

¹*Computational and Applied Mathematics, University of Chicago*

²*Data Science Institute, University of Chicago*

³*Department of Statistics, Department of Computer Science, University of Chicago*

⁴*NSF-Simons National Institute for Theory and Mathematics in Biology*

February 4, 2025

Abstract

Adaptive optimization algorithms—such as Adagrad, Adam, and their variants—have found widespread use in machine learning, signal processing and many other settings. Several methods in this family are not rotationally equivariant, meaning that simple reparameterizations (i.e. change of basis) can drastically affect their convergence. However, their sensitivity to the choice of parameterization has not been systematically studied; it is not clear how to identify a “favorable” change of basis in which these methods perform best. In this paper we propose a reparameterization method and demonstrate both theoretically and empirically its potential to improve their convergence behavior. Our method is an orthonormal transformation based on the *expected gradient outer product* (EGOP) matrix, which can be approximated using either full-batch or stochastic gradient oracles. We show that for a broad class of functions, the sensitivity of adaptive algorithms to choice-of-basis is influenced by the decay of the EGOP matrix spectrum. We illustrate the potential impact of EGOP reparameterization by presenting empirical evidence and theoretical arguments that common machine learning tasks with “natural” data exhibit EGOP spectral decay.

1 Introduction

Adaptive optimization algorithms are popular methods in modern machine learning [8]. Optimizers in this family include the seminal Adagrad and Adam algorithms as well as variants such as AdamW, Adadelta, and Adamax [19, 23, 29, 38]. These iterative algorithms are termed “adaptive” because they maintain and update different learning rates for each coordinate in parameter space.¹ Despite their popularity, fully understanding the impact these adaptive learning rates have on convergence remains an area of ongoing research [18, 22, 24]. Notably, the coordinate-wise learning rates make these methods sensitive to orthonormal reparameterization, distinguishing them from equivariant methods like gradient descent, which have the same convergence rate regardless of orthonormal reparameterization.

Orthonormal reparameterizations correspond to full-dimensional changes of basis, and include seemingly benign transformations such as rotations of the loss landscape about the origin. The sensitivity of adaptive algorithms to rotation means that changes of basis can affect the rate of convergence to local minima, and even impact the generalization properties of the obtained solutions in the presence of non-convex landscapes.

Given the sensitivity of these ubiquitous optimization methods to choice of basis, we pose the following research question:

¹In this work we focus on adaptive algorithms with diagonal pre-conditioners, which correspond to the standard implementation of Adagrad, Adam, and variants in popular software packages. Full-matrix Adagrad, proposed by Duchi et al. [12], is equivariant but requires computing a matrix root on every iteration and is thus rarely used in practice. We also note that adaptive methods may use learning rates for blocks of coordinates, rather using one learning rate for each individual coordinate.

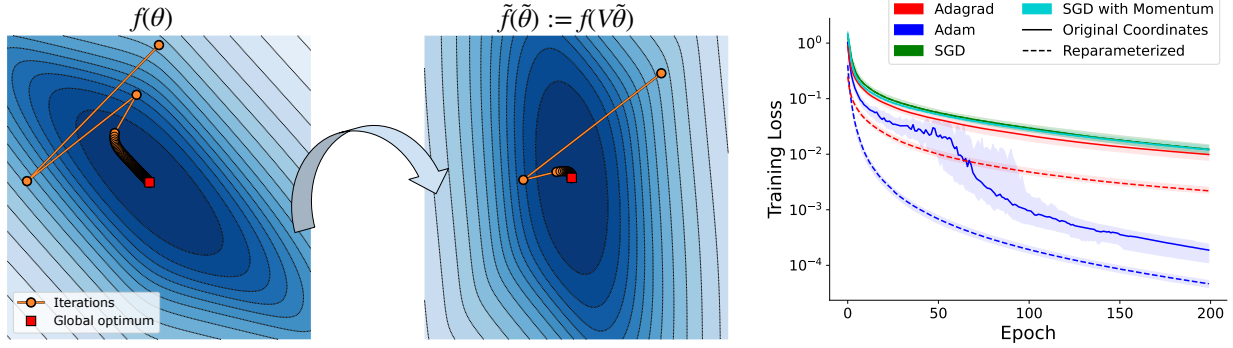


Figure 1: (Left) Visualization of optimizing a two-dimensional log-sum-exp objective (7) using Adagrad in both original coordinates and under EGOP reparameterization. In the EGOP eigenbasis, the primary directions of function variation are axis-aligned. Experimental details in Appendix D.3. (Right) Negative log-likelihood loss over epochs from training a 2-layer ReLU network in 2.4k dimensions to classify handwritten digits using Adam, Adagrad, SGD, and SGD with momentum, in both original coordinates and under reparameterization. Equivariant methods (e.g. SGD) exhibit no change under reparameterization. See discussion in Section 6.

When using an adaptive algorithm, in what settings and to what extent can change-of-basis improve optimization?

In this work, we address this research question by identifying geometric properties of loss functions that govern the sensitivity of adaptive algorithms to change-of-basis. We propose a reparameterization procedure based the *expected gradient outer product* (EGOP) matrix, which captures these geometric properties, and show this reparameterization can improve convergence of adaptive methods. The geometric properties identified in this work—namely, strong decay of the EGOP eigenvalues—have been observed in a variety of machine learning objectives [26, 31, 39]. We include both empirical evidence and theoretical arguments suggesting that these properties arise when using natural data.

Contributions We show that for a large class of objectives, the proposed reparameterization procedure can improve the convergence of adaptive optimization algorithms. Our main contributions are as follows:

- We characterize a class of objective functions for which reparameterization can reduce the number of iterations required for adaptive algorithms to converge to first-order stationary points.
- For these functions, we identify a choice of basis in which adaptive algorithms will perform well, and we propose an approximation procedure that only requires access to a (stochastic) gradient oracle, rather than analytical knowledge about the loss function. This procedure is defined in Section 2.
- We develop theory that proves the proposed reparameterization endows adaptive algorithms with improved convergence guarantees, quantified in terms of the spectrum of the EGOP matrix. Our main results are discussed in Section 3.
- We empirically examine the performance of this procedure and find that the proposed reparameterization improves the convergence of both Adagrad and Adam, for convex and nonconvex objective functions, and machine learning loss functions corresponding to both natural and synthetic data. We present empirical results in Section 6.

1.1 Related Work

Our work intersects with research on theoretical guarantees for adaptive algorithms, the role of orthogonal rotations in algorithmic performance, and the geometry of machine learning objectives with natural data. Here we present a concise overview of relevant works, and include an expanded discussion in Section F of the supplementary material.

Geometric Sensitivity of Adaptive Methods A large body of research has been devoted to understanding when adaptive algorithms’ per-coordinate learning rates confer a benefit over (stochastic) gradient descent ((S)GD). Recently, there has been renewed interest in distinguishing the properties of adaptive algorithms versus SGD, as several empirical studies suggest that adaptive methods outperform SGD when training transformer models [20, 39]. Traditional analyses of adaptive algorithms establish regret bounds for online convex optimization [12, 17]. More recent work establishes convergence rates for smooth, non-convex objectives in terms of the ℓ_2 norm of the gradient [11, 35]. However, because SGD is known to have optimal convergence rates in these settings, these theoretical results only show that adaptive algorithms achieve rates matching those of SGD.

In order to understand when adaptive algorithms enjoy provably stronger guarantees than SGD, a recent line of work studies convergence under refined geometric assumptions, with particular emphasis on assumptions that are *not* rotationally invariant [18, 22, 37]. Xie et al. [37] establish convergence guarantees in terms of the ℓ_∞ smoothness constant of the objective and show experimentally that rotationally invariant geometric assumptions do not suffice to capture settings when Adam out-performs SGD. Jiang et al. [18] and Liu et al. [22] study convergence of Adagrad on objectives that are *coordinate-wise smooth*, defined in Section 1.2. Both works prove similar convergence guarantees for Adagrad; they measure convergence with the gradient ℓ_1 norm, rather than ℓ_2 , because in this regime they can prove a gap between convergence guarantees for Adagrad versus SGD that is consistent with the advantage exhibited by adaptive methods in certain settings [18]. Jiang et al. [18] show that when objective functions exhibit certain geometric properties, Adagrad enjoys ℓ_1 convergence upper bounds that are lower than corresponding lower bounds on SGD’s convergence by a factor of d [18]. Our analysis builds on that of Jiang et al. [18] and Liu et al. [22]; they show that the sum of the coordinate-wise smoothness constants governs Adagrad convergence, and we prove that EGOP reparameterization decreases this value by a factor as large as $1/d$.

Change-of-Basis for Adaptive Algorithms Recent works propose that using different orthonormal transformations with Adam and its variants can reduce computational costs and improve performance in neural network training [24, 34, 40]. Gupta et al. [15] introduced Shampoo, an efficient preconditioning method for optimizing tensor spaces. Vyas et al. [34] formalized a connection between Shampoo and a variant of Adagrad, leading to a new proposed method called SOAP. Designed for training neural networks, SOAP computes an orthonormal reparameterization based on the singular vectors of the matrix-valued network gradients and performs optimization in this basis. Vyas et al. [34] empirically examine the performance of SOAP and find that it outperforms both Adam and Shampoo in LLM pre-training. Zhao et al. [40] propose GaLore, a method that simultaneously performs reparameterization and dimensionality reduction. GaLore computes a similar orthogonal basis to that used in SOAP, but instead of a full-dimensional change-of-basis GaLore retains only leading basis vectors in order to reduce dimension [40]. Maes et al. [24] empirically study Adam’s rotational sensitivity and examine the power of existing geometric assumptions (such as those leveraged by Xie et al. [37]) to explain Adam’s performance when training transformer architectures. They propose an orthonormal reparameterization, similar to those used by SOAP and GaLore, and show empirically that this can improve Adam’s performance [24].

SOAP and GaLore are empirically powerful tools, but their convergence properties are not fully understood. The results in this work may lead to new ways to analyze the performance of SOAP and GaLore. See Appendix E for further discussion of the main distinctions between our proposed reparameterization methods and SOAP/GaLore.

Outside of training neural networks, several works have considered data-driven dimensionality reduction methods for optimizing more general objectives with low-rank EGOP matrices [3, 7]. These procedures target objectives with exact low-rank structure, while our method can improve convergence of adaptive algorithms even when the EGOP matrix has strong spectral decay but is full-rank.

EGOP Structure in Machine Learning Increasing empirical evidence across a wide range of applications, including language modeling and image classification, suggests that empirical loss functions used for training machine learning models are approximately low-rank—meaning that the functions vary strongly in only a small subset of directions in parameter space Papyan [26], Sagun et al. [31], Zhang et al. [39]. Such approximate low-rank structure can be detected and analyzed using active subspace methods. Many active subspace methods leverage the EGOP matrix (sometimes referred to as the average gradient outer product

(AGOP) matrix), which we define in Section 2 [6]. Recently, there has been growing interest in the EGOP and in the use of active subspace methods in machine learning research [9, 25, 28, 41]. Radhakrishnan et al. [28] provide theoretical and empirical evidence that the weight matrices of deep neural networks trained with gradient descent correlate strongly with a kind of EGOP matrix.²

1.2 Notation

For a vector $\theta \in \mathbb{R}^d$, we denote its i^{th} entry by $\theta(i)$. We denote the inner product on \mathbb{R}^d by $\langle \cdot, \cdot \rangle$, and let $\|\cdot\|_p$ denote the vector p -norm on \mathbb{R}^d , with $\|\theta\|_\infty \stackrel{\text{def}}{=} \max_i |\theta(i)|$. Given a matrix $A \in \mathbb{R}^{m \times n}$, we write $\|A\|_F$ for its *Frobenius* norm and $\|A\|_{\text{op}} \stackrel{\text{def}}{=} \sup_{\|\theta\|_2=1} \|A\theta\|_2$ for its *spectral* norm. Given a PSD matrix $H \in \mathbb{R}^{d \times d}$, we denote the norm $\|\theta\|_H \stackrel{\text{def}}{=} \sqrt{\langle \theta, H\theta \rangle}$. For a matrix $A \in \mathbb{R}^{n \times m}$, we denote the vectorization of A by $\text{vec}(A) \in \mathbb{R}^{nm}$.

We obtain guarantees in terms of the *coordinate-wise smoothness constants* of the objective $f(\cdot)$. Following Jiang et al. [18] and Liu et al. [22], we say that a function f satisfies coordinate wise smoothness with constants $L_1, \dots, L_d > 0$ if the following holds for all $\theta_1, \theta_2 \in \mathbb{R}^d$:

$$|f(\theta_1) - f(\theta_2) - \langle \nabla f(\theta_2), \theta_1 - \theta_2 \rangle| \leq \frac{1}{2} \|\theta_1 - \theta_2\|_L^2, \quad (1)$$

where $L = \text{diag}(L_1, \dots, L_d)$. We will denote by L_f the sum of these constants for a particular function $f(\cdot)$: $L_f \stackrel{\text{def}}{=} \sum_{i=1}^d L_i$.

2 EGOP Reparameterization

Given a function $f : \mathbb{R}^d \rightarrow \mathbb{R}$ and a sampling distribution ρ , the expected gradient outer product of $f(\cdot)$ with respect to ρ is defined as

$$\text{EGOP}(f) \stackrel{\text{def}}{=} \mathbb{E}_{\theta \sim \rho} [\nabla f(\theta) \nabla f(\theta)^\top].$$

As $f : \mathbb{R}^d \rightarrow \mathbb{R}$, the EGOP is a $d \times d$ symmetric matrix, and it is positive semi-definite because it is an expectation over PSD matrices. We denote its eigendecomposition by

$$\text{EGOP}(f) = V \Lambda V^\top$$

where $V \in \mathbb{R}^{d \times d}$ is an orthonormal matrix. The EGOP eigenbasis captures key geometric qualities of the function $f(\cdot)$. When the sampling distribution ρ is isotropic, the leading eigenvectors of the EGOP matrix capture the directions of greatest variation in $f(\cdot)$, whereas the eigenspaces of the smallest eigenvalues are directions along which $f(\cdot)$ does not vary strongly: for any eigenpair (λ_i, v_i) of $\text{EGOP}(f)$,

$$\lambda_i = \mathbb{E}_{\theta \sim \rho} [\langle \nabla f(\theta), v_i \rangle^2]. \quad (2)$$

In this work, we compare how adaptive optimization algorithms perform when optimizing $f(\cdot)$ versus the reparameterized function $\tilde{f} : \mathbb{R}^d \rightarrow \mathbb{R}$ defined $\tilde{f}(\tilde{\theta}) \stackrel{\text{def}}{=} f(V\tilde{\theta})$. For any f , the objective $\tilde{f}(\cdot)$ can be approximated by empirically estimating the EGOP via Monte Carlo sampling and forming the eigenvectors of the empirical EGOP matrix, as summarized in Algorithm 1.

Note that as V is orthogonal, any solution $\tilde{\theta}$ obtained by optimizing $\tilde{f}(\cdot)$ can be transformed into a solution in original coordinates as $\theta \stackrel{\text{def}}{=} V\tilde{\theta}$, which satisfies $f(\theta) = \tilde{f}(\tilde{\theta})$.

Algorithm 1 requires a user-specified sampling distribution ρ . Our guarantees in Section 3 require that ρ be isotropic and that its scale is large enough with respect to the norm of some local minimum of $f(\cdot)$. In Section 6, we present empirical results when the EGOP is estimated with ρ a standard Gaussian, and when ρ is defined by common neural network initialization distributions [13].

²In Mallinar et al. [25], Radhakrishnan et al. [28] and Zhu et al. [41], the EGOP is defined using the gradient with respect to the *input data* instead of the optimization parameters.

Algorithm 1 Reparameterization by EGOP Eigenbasis

Input: M number of gradient samples, distribution ρ .
Generate $\{\theta_i\}_{i=1}^M \sim \rho$ i.i.d.
Form empirical EGOP $\hat{P} = \frac{1}{M} \sum_{i=1}^M \nabla f(\theta_i) \nabla f(\theta_i)^\top$
Form eigendecomposition $V \Lambda V^\top = \hat{P}$
Define function $\tilde{f}(\cdot) = f \circ V$
Optimize $\tilde{f}(\cdot)$ with adaptive algorithm of choice.
Output: $\tilde{\theta} \in \mathbb{R}^d$ the result of optimizing $\tilde{f}(\cdot)$.

3 Convergence Guarantees under EGOP Reparameterization

In this section, we show that for objectives with strong EGOP spectral decay, reparameterization by the EGOP eigenbasis can improve convergence guarantees for adaptive methods. We consider convergence guarantees for Adagrad, and relate the improvement obtained through reparameterization by the EGOP eigenbasis to the *stable rank*³ of f :

$$\text{sr}_f \stackrel{\text{def}}{=} \frac{\sum_{i=1}^d \sqrt{\lambda_i(\text{EGOP}(f))}}{\sqrt{\lambda_{\max}(\text{EGOP}(f))}}. \quad (3)$$

Functions with strong EGOP spectral decay will have constant stable rank (tending towards 1 as spectral decay increases), while functions without EGOP spectral decay will have a stable rank that scales with d .

We now introduce the main assumptions for our theoretical results. Setting the stage, we consider a twice-differentiable objective $f : \mathbb{R}^d \rightarrow \mathbb{R}$, a sampling distribution $\rho(\cdot)$ and fix a local minimum θ^* .

Assumption 1. *The sampling distribution $\rho(\cdot)$ is mean-zero, isotropic, and sufficiently “spread out”; i.e.,*

$$\mathbb{E}_{\theta \sim \rho}[\theta \theta^\top] = c^2 \mathbb{I} \quad \text{for some } c \geq \|\theta^*\|.$$

Assumption 2. *The Hessian of $f(\cdot)$ is H -Lipschitz:*

$$\|\nabla^2 f(\theta_1) - \nabla^2 f(\theta_2)\|_{\text{op}} \leq H \|\theta_1 - \theta_2\|, \text{ for all } \theta_1, \theta_2.$$

Under the above assumptions, we show that EGOP spectral decay governs the improvements conferred by EGOP reparameterization.

Theorem 3 (Informal). *Consider a function $f : \mathbb{R}^d \rightarrow \mathbb{R}$ and a sampling distribution ρ satisfying Assumptions 1 and 2. Let $\Delta_f \stackrel{\text{def}}{=} f(\theta_0) - \inf_{\theta \in \mathbb{R}^d} f(\theta)$ for some initialization point θ_0 , and assume Δ_f is finite. Consider optimizing $f(\cdot)$ with Adagrad using step size η . Let $\{\tilde{\theta}_t\}_{t=1}^T$ denote the iterates produced by optimizing the reparameterizing objective $\tilde{f} \stackrel{\text{def}}{=} f \circ V$ using Adagrad initialized at $V^\top \theta_0$, where V denotes the eigenbasis of $\text{EGOP}(f)$. Let $\beta \stackrel{\text{def}}{=} \|v_1\|_1^2/d$ for v_1 the leading EGOP eigenvector. Then if the value H in Assumption 2 is sufficiently small, reparameterized Adagrad convergence is bounded by*

$$\frac{1}{T} \sum_{t=1}^T \|\nabla \tilde{f}(\tilde{\theta}_t)\|_1 = \tilde{O} \left(\frac{\text{sr}_f}{\beta d} \cdot \frac{\eta L_f}{\sqrt{T}} + \frac{\Delta_f}{\eta \sqrt{T}} \right)$$

where sr_f denotes the stable rank (3).

We compare the above bound with the convergence guarantee for Adagrad in original coordinates initialized at θ_0 :

$$\frac{1}{T} \sum_{t=1}^T \|\nabla f(\theta_t)\|_1 = \tilde{O} \left(\frac{\eta L_f}{\sqrt{T}} + \frac{\Delta_f}{\eta \sqrt{T}} \right)$$

³We call this quantity the stable rank because of the connection to the stable rank considered in numerical linear algebra; the ratio in (3) is related to $\|G\|_* / \|G\|_{\text{op}}$, where G denotes the empirical gradient bundle matrix $[\nabla f(\theta_1), \dots, \nabla f(\theta_M)] \in \mathbb{R}^{d \times M}$ and $\|\cdot\|_*$ denotes the nuclear norm. This ratio is often referred to in literature as the *stable* or *effective rank* of G [5, 30].

where $\{\theta_t\}_{t=1}^T$ denote the iterates produced by the algorithm in original coordinates, and the term L_f appearing in both this bound and in Theorem 3 denotes the sum of the coordinate-wise smoothness constants of $f(\cdot)$ in original coordinates [18, 22].

When $f(\cdot)$ has strong EGOP spectral decay and dense leading eigenvectors, Theorem 3 implies the convergence bounds for reparameterized Adagrad are much stronger: in these settings, $\text{sr}_f/(\beta d) = O(1/d)$. We defer the proof of Theorem 3 to Appendix A.1.1. We show that the two properties of the EGOP emphasized in this result, namely low stable rank and dense leading eigenvectors, are satisfied empirically in Section 4. Many naturally-motivated objectives in machine learning satisfy Assumption 2, including loss functions used in logistic regression, over-parameterized matrix factorization, and training of multilayer linear networks. We bound the Lipschitz constants of the Hessians of these objectives in Appendix A.1.2.

Our guarantee in Theorem 3 holds for any step size. If one chooses the step size η optimally in order to minimize the upper bounds, the convergence guarantee for the reparameterized iterates becomes $\tilde{O}\left(\sqrt{\frac{\text{sr}_f}{\beta d} \cdot \frac{L_f \Delta_f}{T}}\right)$, while the convergence bound in original coordinates becomes $\tilde{O}\left(\sqrt{\frac{L_f \Delta_f}{T}}\right)$. This implies that under such choice of η , reparameterization offers improvement by a factor of $\sqrt{\text{sr}_f/\beta d}$. However, in practice users must select learning rates without a-priori knowledge of the smoothness constants. In these settings η is typically set through hyperparameter tuning. Theorem 3 implies that the optimal step size for reparameterized Adagrad is larger than that of Adagrad in original coordinates by a factor of $\sqrt{\beta d/\text{sr}_f}$. Theorem 3 also implies that for large values of η , reparameterization offers improvement by a factor as large as $\text{sr}_f/(\beta d)$, which agrees with our empirical results in Section 6 showing that reparameterized methods perform even better with larger step sizes (see e.g. Fig. 3b).

The factor $\beta = \|v_1\|_1^2/d$ tends towards 1 as the leading EGOP eigenvector gets denser. For the guarantee to reflect a benefit from reparameterization, it suffices to have $\beta \gg 1/d$ and small stable rank. In Section 4, we empirically verify this property on benchmark image datasets. For simplicity, the guarantee in Theorem 3 only considers the density of v_1 , but more general guarantees can be obtained in terms of the measure $\max_k \max_{\nu \in \{\pm 1\}^d} \lambda_k \sum_{i=1}^d \langle \nu, v_k \rangle^2/d$. Similarly, one can derive generalizations of Theorem 3 for approximate versions of the EGOP eigenbasis; such guarantees will scale with the subspace distance between the EGOP eigenbasis and its approximation.

We measure convergence with respect to the ℓ_1 gradient norm instead of the ℓ_2 norm⁴ because this is the measure by which convergence guarantees for adaptive algorithms can be provably separated from those for SGD [18].

4 EGOP Spectral Decay in Machine Learning

Our analysis in Section 3 shows EGOP spectral decay and dense leading EGOP eigenvectors are sufficient for EGOP reparameterization to improve convergence guarantees for Adagrad. Here we present empirical evidence that these conditions occur in benchmark machine learning objectives, and we discuss theoretical reasons for why natural data results in EGOP spectral decay in real-world problems.

Figure 2 shows the EGOP eigenspectrum for the objective function $f(\cdot)$ from an image classification problem. We use a 2-layer ReLU neural network to predict 10-class probabilities for handwritten digit images from the UCI ML digits dataset (Alpaydin and Kaynak [1]). Here $f(\cdot)$ denotes the negative log-likelihood loss on the training data. Figure 2 shows strong EGOP spectral decay. We plot λ_k/λ_1 for all EGOP eigenvalues λ_k on a logarithmic scale, while the inset zooms in on the leading 100 indices on a linear scale. These plots illustrate roughly exponential eigenvalue decay in regions of the spectrum.

In Appendix C.1, we show that these trends are robust to choice of sampling distribution (see Figure 6). In this appendix we also visualize the eigenspectra of the layer block EGOP matrices, defined in Section 5, for neural networks on both the UCI digits dataset and a subset of the fashionMNIST dataset (see Figure 7) [1, 36]. We observe that the spectral decay illustrated in Fig. 2 persists when considering block EGOP matrices instead of global EGOP matrices, and that this spectral decay occurs across different datasets.

In Appendix C.1, we examine the density of the leading EGOP eigenvectors for a 2-layer ReLU network on the UCI digits dataset. We show that $\beta \geq 0.5$, while for this network the number of parameters d satisfies

⁴We note that as the ℓ_2 norm is upper-bounded by the ℓ_1 norm, the guarantees in Theorem 3 also imply stronger convergence guarantees under reparameterization in terms of the ℓ_2 gradient norm measure.

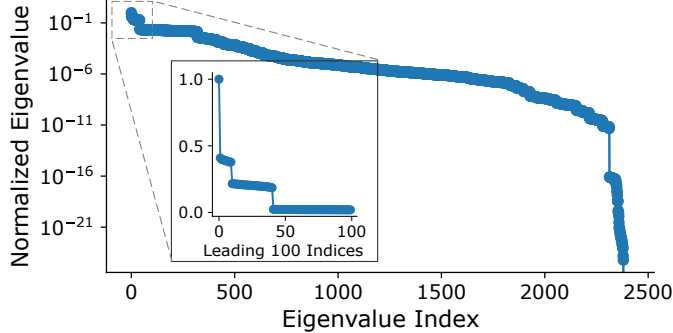


Figure 2: The EGOP eigenspectrum of a 2-layer ReLU network on the UCI handwritten digits dataset. Plot shows ratio λ_k/λ_1 as a function of eigenvalue index k , indexed in decreasing order.

$1/d < 5 \cdot 10^{-4}$ and thus $\beta \gg 1/d$, and we show that several of the leading eigenvectors exhibit similar density (see Fig. 8).

4.1 Natural Data Induces EGOP Spectral Decay

In addition to empirical evidence, simple gradient calculations suggest that natural data may induce EGOP spectral decay in machine learning problems. Many objectives in machine learning can be expressed as $f(\theta) = h(A\theta)$, where $h(\cdot)$ is a loss function and $A \in \mathbb{R}^{n \times d}$ is a data matrix whose rows comprise samples $a_i \in \mathbb{R}^d$. By the chain rule, the EGOP for such objectives satisfies

$$\text{EGOP}(f) = A^\top \mathbb{E}_{\theta \sim \rho} [\nabla_\theta h(A\theta) \nabla_\theta h(A\theta)^\top] A \quad (4)$$

where $\nabla_\theta h(A\theta)$ denotes the gradient $\nabla h(\cdot)$ evaluated at $A\theta$. The above expression shows the EGOP is formed by transforming some PSD matrix M by $A^\top M A$. It suggests that if A has strong spectral decay, this may induce eigenvalue decay in the EGOP matrix. Indeed for many naturally occurring data distributions, the singular values of A exhibit significant decay [32].

The inner PSD matrix in the right hand side of Eq. 4 depends on both A and $h(\cdot)$, so without further assumptions on $h(\cdot)$ it is difficult to precisely characterize the spectral decay induced by the composition with A^\top and A . However, the spectral decay induced by A can be quantified for specific choices of $h(\cdot)$; see Appendix A.2 for some examples.

We note that the density condition $\beta \gg 1/d$ is satisfied with high probability for random unit vectors in high dimensions: in particular, for $v \sim \text{Unif}(S^{d-1})$ where S^{d-1} is the unit sphere in \mathbb{R}^d , with high probability $\|v\|_1^2/d \approx 2/\pi > 0.6$.

5 Heuristics for Scalability

Reparameterization with the EGOP eigenbasis incurs three main sources of additional computation: (1) sampling gradients to estimate the EGOP, (2) forming the EGOP eigenbasis, and (3) storing and applying the change-of-basis matrix to compute values and gradients of $f \circ V$. We outline some implementation details and heuristics that reduce the computational cost and enhance the scalability of the proposed framework. For a more detailed discussion, see Appendix B.

We hypothesize that for functions with strong spectral decay, it suffices to accurately estimate only the leading EGOP eigenvectors. The remaining columns of the matrix V can be completed using any random orthonormal basis for the orthogonal complement of the leading eigenspace. Based on this hypothesis, one can use techniques like randomized SVD [16] to form $V_k \in \mathbb{R}^{d \times k}$, a matrix whose columns contain the estimated k leading eigenvectors of the EGOP, and then append any random orthonormal basis for the complement to produce $V \in \mathbb{R}^{d \times d}$. Alternatively, one can employ a partial basis instead of a full orthonormal basis. GaLore, discussed in Appendix F, uses such a partial basis but requires periodic re-computation of the basis in order

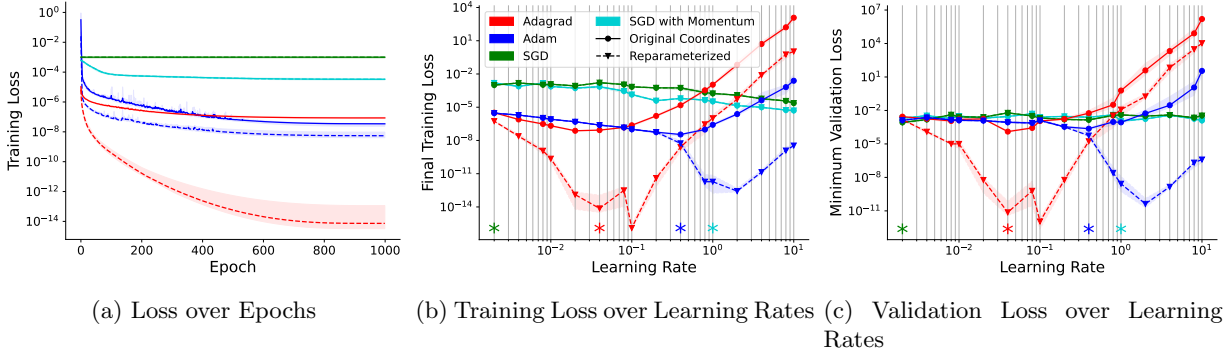


Figure 3: Training multilayer linear networks (6). Both SGD and SGD with momentum are equivariant optimization methods, so their results in original and reparameterized coordinates are exactly superimposed. In Fig. 3c we consider the minimum validation loss achieved over epochs during training. Results are aggregated over 10 independent trials, with traces showing medians and shading indicating 25th-75th quartile. Asterisks indicate the learning rate used for each method in Fig. 3a. Learning rates chosen to minimize validation loss of the algorithm in *original* coordinates.

to achieve good performance [40]. We also note that for functions with strong spectral decay, a conservative number of gradient samples ($M \leq 2d$, where M is the number of samples and d is the number of problem parameters) is empirically sufficient to yield change-of-basis matrices.

The “partial basis” strategy outlined above is one of several possible ways to reduce the cost of storing and/or applying a change of basis. Other heuristics include structured or factorized approximations of V . One can group the optimization variables in the vector θ into subsets $\{S_i\}_{i=1}^L$ and perform *block reparameterization*. For each subset, we obtain a separate change-of-basis matrix $V^{(i)} \in \mathbb{R}^{|S_i| \times |S_i|}$ via the eigenvectors of the *block* EGOP matrix,

$$\text{EGOP}^{(i)} \stackrel{\text{def}}{=} \frac{1}{M} \sum_{k=1}^M \nabla_{S_i} f(\theta_k) \nabla_{S_i} f(\theta_k)^\top \quad (5)$$

where $\nabla_{S_i} f(\theta_k) \in \mathbb{R}^{|S_i|}$ is the vector of partial derivatives of f w.r.t. the entries in S_i , and the points $\{\theta_k\}_{k=1}^M \stackrel{\text{i.i.d.}}{\sim} \rho$. Block reparameterization is well-suited to multilayer neural networks, where each layer forms a parameter block; further savings can be obtained by only reparameterizing a subset of blocks (see Section 6). Another approach is a Kronecker-product factorization, where one finds matrices $V_1 \in \mathbb{R}^{m_1 \times n_1}$, $V_2 \in \mathbb{R}^{m_2 \times n_2}$ for $m_1 m_2 = n_1 n_2 = d$ such that $V \approx V_1 \otimes V_2$. This reduces the storage cost from d^2 to $m_1 n_1 + m_2 n_2$, and is similar to the method proposed by Vyas et al. [34].

6 Experimental Results

We examine the impact of EGOP reparameterization in a variety of settings. We compare how the seminal adaptive algorithms, Adagrad and Adam, perform when optimizing functions in original coordinates versus under reparameterization by the empirical EGOP eigenbasis, both as described in Algorithm 1 and with the block reparameterization described in Section 5. We include comparisons to equivariant iterative optimization methods, namely (stochastic) gradient descent and (S)GD with momentum. When comparing methods, we always choose equivalent initializations: when a method in original coordinates is initialized at θ_0 , chosen randomly, the reparameterized method is initialized at $V^\top \theta_0$. Full experimental details are in Appendix D.

Linear Feedforward Networks We examine the impact of EGOP reparameterization on training 3-layer fully-connected linear feedforward networks using synthetic data. We consider parameters

$$\theta = [\text{vec}(W_1), \text{vec}(W_2), \text{vec}(W_3)]$$

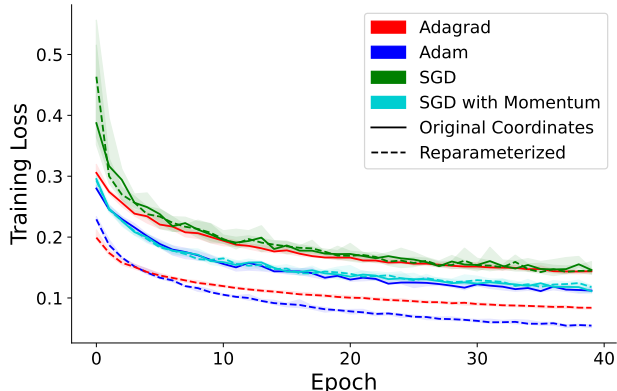


Figure 4: Block EGOP reparameterization on fashionMNIST. Results are aggregated over independent trials corresponding to different random initializations. Medians are plotted as traces, and shaded regions indicate the 25th-75th percentiles. Each algorithm (Adagrad, Adam, etc) uses the same learning rate for both coordinate systems. Full details in Appendix D.

where $W_1 \in \mathbb{R}^{50 \times 10}$, $W_2 \in \mathbb{R}^{30 \times 50}$, $W_3 \in \mathbb{R}^{10 \times 30}$. We train by minimizing loss function

$$f(\theta) = \|W_3 W_2 W_1 A - Y\|_F^2 / n_{\text{samples}} \quad (6)$$

where $A \in \mathbb{R}^{10 \times n_{\text{samples}}}$, and $Y = M^* A$ for $M^* \in \mathbb{R}^{10 \times 10}$ drawn from a standard Gaussian distribution. We induce spectral decay in $\text{EGOP}(f)$ by generating A with singular values $\sigma_k(A) = k^{-2}$ and random singular vectors. We use minibatched stochastic gradient samples throughout. Full experimental details are deferred to Appendix D.

In Figure 3 we study the impact of global EGOP reparameterization (Algorithm 1). Fig. 3a shows training loss over epochs in original coordinates and under reparameterization. Reparameterized Adagrad and reparameterized Adam achieve significantly lower final training loss and faster convergence than their counterparts in original coordinates. The adaptive methods also outperform the equivariant methods (SGD and SGD with momentum) in both reparameterized and original coordinates.

Fig. 3b demonstrates the robustness of these results across learning rates. Asterisks along the x-axis indicate the learning rates used in Fig. 3a. Fig. 3c confirms that the improved minimization of the training loss enabled by reparameterization does not lead to over-fitting. The figure plots validation loss achieved as a function of learning rate, and shows that reparameterization enables adaptive methods to achieve better performance on validation data.

In Appendix C.2, we compare the above results to those obtained when performing block reparameterization, as described in Section 5. We also visualize the impact of reparameterizing only the first layer of the network, corresponding to the parameters in W_1 in Eq. 6. We find that both block-reparameterized Adagrad and Adam achieve lower final training loss than their counterparts in original coordinates. For Adagrad, reparameterizing only the first layer confers a benefit comparable to block reparameterizing all layers, while for Adam reparameterizing the first layer alone provides only a marginal benefit over original coordinates.

ReLU Networks for Image Classification We examine the impact of EGOP reparameterization when training networks to perform image classification using real-world data. We consider two benchmark image classification datasets: the UCI hand-written digits dataset (8×8 pixel images), and the fashionMNIST dataset (28×28 pixel images of clothing) [1, 36]. For fashionMNIST, we down-sample images to 14×14 pixels and restrict our dataset to samples from the first four classes; we do this in order to reduce the problem size to a setting where we can implement procedures most consistent with our theory. We train multilayer fully-connected ReLU networks to perform image classification on each dataset by minimizing the cross-entropy loss. We perform block EGOP reparameterization, as described in Section 5. We use stochastic minibatch gradients throughout. For these experiments, the number of gradient samples drawn equals the number of model weight parameters. For full experimental details, see Appendix D.

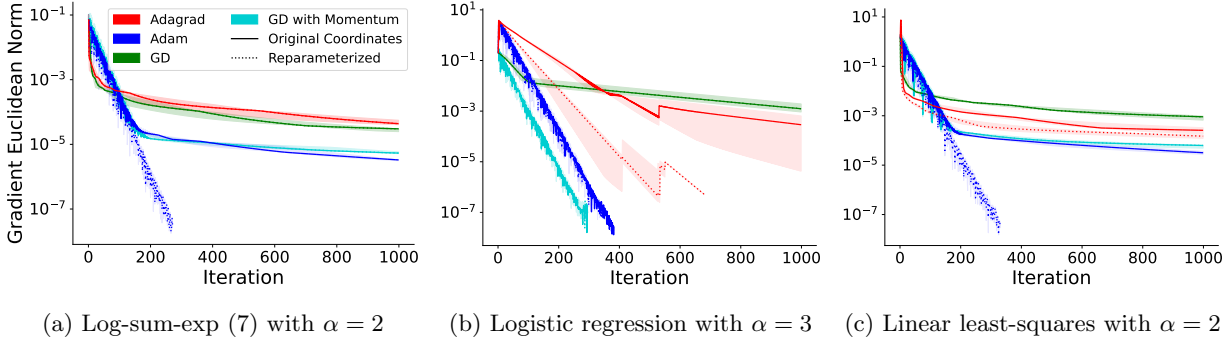


Figure 5: Gradient Euclidean norm of solution at t^{th} iterate. Learning rates were chosen to minimize loss of the algorithm in original coordinates. We induce EGOP spectral decay by choice of data matrix A with singular values $\sigma_k(A) = k^{-\alpha}$. As noted in the prose, in some plots the dotted traces coincide with the solid and are thus not visible (Adagrad in Fig. 5a, Adam in Fig. 5a).

Fig. 1 (right) and Fig. 4 plot training loss by epoch for the UCI digits dataset and fashionMNIST respectively. On both datasets, the reparameterized adaptive methods out-perform their counterparts in original coordinates, and reparameterized Adam achieves the best performance. We note that all methods achieve comparable accuracy on held-out data: median validation accuracy for all methods ranges between 95-96% for the digits dataset, and between 93-94% for fashionMNIST. This indicates that the improved training produced by reparameterization did not lead to over-fitting. In Appendix C.2, we report test accuracy and show that these results are robust to choice of learning rate.

Convex Objectives In addition to training neural networks, which is a primary application of adaptive optimization algorithms, we also study reparameterization for convex optimization. Fig. 5a shows the result of minimizing

$$f(\theta) = \log \left(\sum_{i=1}^n \exp(\langle a_i, \theta \rangle - y_i)^2 \right), \quad (7)$$

where $a_i \in \mathbb{R}^d$ denote vectors of observations and $y_i \stackrel{\text{def}}{=} \langle a_i, \theta^* \rangle$ for ground truth θ^* . We also plot results from minimizing logistic regression objectives (Fig. 5b) and linear least-squares objectives (Fig. 5c) arising from problems with data matrices $A \in \mathbb{R}^{n \times d}$. For all convex objectives, we induce EGOP spectral decay by choosing matrices A with singular value decay. For these objectives, we estimate the EGOP and perform optimization using noiseless (full-batch) gradients.

Fig. 5 demonstrates that EGOP reparameterization can improve convergence of adaptive algorithms to global minima of convex objectives. For the log-sum-exp objective (Fig. 5a), reparameterization accelerates Adam’s convergence, but has no impact on Adagrad. In Appendix C.2, we show that if learning rates are tuned separately for each coordinate setting, reparameterized Adagrad can use a larger learning rate and thus converge more quickly than Adagrad in original coordinates. For logistic regression (Fig. 5b), Adam achieves comparable performance in both coordinate settings, while gradient descent with momentum outperforms all other methods. Notably, methods with momentum excel for this objective, and reparameterization boosts the performance of Adagrad (which does not use momentum), making it competitive with the momentum-based optimizers. For linear least-squares (Fig. 5c), reparameterization improves the performance of both Adam and Adagrad. As with log-sum-exp, Appendix C.2 shows that if learning rates are tuned separately for each coordinate system, then reparameterized Adagrad can achieve even better performance.

7 Conclusions and Limitations

In this work, we have shown through both analysis and experiments that EGOP reparameterization can improve convergence of adaptive algorithms. There may be opportunities for future work to explore other reparameterizations and additional hyperparameter tuning which we have not examined in this work. One

limitation of this work is the engineering required for scalability, as discussed in Section 5. Fully characterizing the trade-off between improved convergence and the up-front cost of reparameterization remains a direction for future research. Another interesting direction is whether competing explanations for Adam’s empirical out-performance of SGD on LLM training—in terms of achieving lower training error and converging more quickly—may be unified through the lens of EGOP spectral decay [20, 39].

Acknowledgments

We thank Lorenzo Orecchia for several helpful conversations about the role of smoothness in analyzing related methods. We gratefully acknowledge the support of AFOSR FA9550-18-1-0166, NSF DMS-2023109, DOE DE-SC0022232, the NSF-Simons National Institute for Theory and Mathematics in Biology (NITMB) through NSF (DMS-2235451) and Simons Foundation (MP-TMPS-00005320), and the Margot and Tom Pritzker Foundation. AD gratefully acknowledges the support of NSF DGE 2140001.

References

- [1] E. Alpaydin and C. Kaynak. Optical Recognition of Handwritten Digits. UCI Machine Learning Repository, 1998. DOI: <https://doi.org/10.24432/C50P49>.
- [2] J. Bradbury, R. Frostig, P. Hawkins, M. J. Johnson, C. Leary, D. Maclaurin, G. Necula, A. Paszke, J. VanderPlas, S. Wanderman-Milne, and Q. Zhang. JAX: composable transformations of Python+NumPy programs, 2018. URL <http://github.com/google/jax>.
- [3] C. Cartis, X. Liang, E. Massart, and A. Otemissov. Learning the subspace of variation for global optimization of functions with low effective dimension. *arXiv preprint arXiv:2401.17825*, 2024.
- [4] X. Chen and E. Hazan. Open problem: Black-box reductions and adaptive gradient methods for nonconvex optimization. In S. Agrawal and A. Roth, editors, *Proceedings of Thirty Seventh Conference on Learning Theory*, volume 247 of *Proceedings of Machine Learning Research*, pages 5317–5324. PMLR, 30 Jun–03 Jul 2024. URL <https://proceedings.mlr.press/v247/chen24e.html>.
- [5] H.-H. Chou, C. Gieshoff, J. Maly, and H. Rauhut. Gradient descent for deep matrix factorization: Dynamics and implicit bias towards low rank. *Applied and Computational Harmonic Analysis*, 68: 101595, 2024.
- [6] P. G. Constantine. *Active subspaces: Emerging ideas for dimension reduction in parameter studies*. SIAM, 2015.
- [7] R. Cosson, A. Jadbabaie, A. Makur, A. Reisizadeh, and D. Shah. Low-Rank Gradient Descent. *IEEE Open Journal of Control Systems*, 2023.
- [8] B. Crew. Google Scholar reveals its most influential papers for 2020, Jul 2020.
- [9] C. Cui, K. Zhang, T. Daulbaev, J. Gusak, I. Oseledets, and Z. Zhang. Active subspace of neural networks: Structural analysis and universal attacks. *SIAM Journal on Mathematics of Data Science*, 2(4):1096–1122, 2020.
- [10] DeepMind, I. Babuschkin, K. Baumli, A. Bell, S. Bhupatiraju, J. Bruce, P. Buchlovsky, D. Budden, T. Cai, A. Clark, I. Danihelka, A. Dedieu, C. Fantacci, J. Godwin, C. Jones, R. Hemsley, T. Hennigan, M. Hessel, S. Hou, S. Kapturowski, T. Keck, I. Kemaev, M. King, M. Kunesch, L. Martens, H. Merzic, V. Mikulik, T. Norman, G. Papamakarios, J. Quan, R. Ring, F. Ruiz, A. Sanchez, L. Sartran, R. Schneider, E. Sezener, S. Spencer, S. Srinivasan, M. Stanojević, W. Stokowiec, L. Wang, G. Zhou, and F. Viola. The DeepMind JAX Ecosystem, 2020. URL <http://github.com/google-deepmind>.
- [11] A. Défossez, L. Bottou, F. Bach, and N. Usunier. A Simple Convergence Proof of Adam and Adagrad. *arXiv preprint arXiv:2003.02395*, 2020.

- [12] J. Duchi, E. Hazan, and Y. Singer. Adaptive subgradient methods for online learning and stochastic optimization. *Journal of Machine Learning Research*, 12(7), 2011.
- [13] X. Glorot and Y. Bengio. Understanding the difficulty of training deep feedforward neural networks. In *Proceedings of the thirteenth international conference on artificial intelligence and statistics*, pages 249–256. JMLR Workshop and Conference Proceedings, 2010.
- [14] G. H. Golub. Some modified matrix eigenvalue problems. *SIAM Review*, 15(2):318–334, 1973.
- [15] V. Gupta, T. Koren, and Y. Singer. Shampoo: Preconditioned stochastic tensor optimization. In *International Conference on Machine Learning*, pages 1842–1850. PMLR, 2018.
- [16] N. Halko, P.-G. Martinsson, and J. A. Tropp. Finding structure with randomness: Probabilistic algorithms for constructing approximate matrix decompositions. *SIAM Review*, 53(2):217–288, 2011.
- [17] E. Hazan et al. Introduction to online convex optimization. *Foundations and Trends® in Optimization*, 2(3-4):157–325, 2016.
- [18] R. Jiang, D. Maladkar, and A. Mokhtari. Convergence analysis of adaptive gradient methods under refined smoothness and noise assumptions. *arXiv preprint arXiv:2406.04592*, 2024.
- [19] D. P. Kingma and J. Ba. Adam: A method for stochastic optimization, 2017. URL <https://arxiv.org/abs/1412.6980>.
- [20] F. Kunstner, R. Yadav, A. Milligan, M. Schmidt, and A. Bietti. Heavy-tailed class imbalance and why Adam outperforms gradient descent on language models. *arXiv preprint arXiv:2402.19449*, 2024.
- [21] S. Z. Ling, N. Sharp, and A. Jacobson. Vectoradam for rotation equivariant geometry optimization. *Advances in Neural Information Processing Systems*, 35:4111–4122, 2022.
- [22] Y. Liu, R. Pan, and T. Zhang. AdaGrad under Anisotropic Smoothness. *arXiv preprint arXiv:2406.15244*, 2024.
- [23] I. Loshchilov and F. Hutter. Decoupled weight decay regularization, 2019. URL <https://arxiv.org/abs/1711.05101>.
- [24] L. Maes, T. H. Zhang, A. Jolicoeur-Martineau, I. Mitliagkas, D. Scieur, S. Lacoste-Julien, and C. Guille-Escuret. Understanding Adam Requires Better Rotation Dependent Assumptions. *arXiv preprint arXiv:2410.19964*, 2024.
- [25] N. Mallinar, D. Beaglehole, L. Zhu, A. Radhakrishnan, P. Pandit, and M. Belkin. Emergence in non-neural models: grokking modular arithmetic via average gradient outer product. *arXiv preprint arXiv:2407.20199*, 2024.
- [26] V. Pappas. The full spectrum of deepnet Hessians at scale: Dynamics with SGD training and sample size. *arXiv preprint arXiv:1811.07062*, 2018.
- [27] A. Paszke, S. Gross, S. Chintala, G. Chanan, E. Yang, Z. DeVito, Z. Lin, A. Desmaison, L. Antiga, and A. Lerer. Automatic differentiation in PyTorch. In *NIPS-W*, 2017.
- [28] A. Radhakrishnan, D. Beaglehole, P. Pandit, and M. Belkin. Mechanism of feature learning in deep fully connected networks and kernel machines that recursively learn features. *arXiv preprint arXiv:2212.13881*, 2022.
- [29] S. J. Reddi, S. Kale, and S. Kumar. On the Convergence of Adam and Beyond, 2019. URL <https://arxiv.org/abs/1904.09237>.
- [30] M. Rudelson and R. Vershynin. Sampling from large matrices: An approach through geometric functional analysis. *Journal of the ACM (JACM)*, 54(4):21–es, 2007.

- [31] L. Sagun, U. Evci, V. U. Guney, Y. Dauphin, and L. Bottou. Empirical analysis of the hessian of over-parametrized neural networks. *arXiv preprint arXiv:1706.04454*, 2017.
- [32] M. Udell and A. Townsend. Why are big data matrices approximately low rank? *SIAM Journal on Mathematics of Data Science*, 1(1):144–160, 2019.
- [33] P. Virtanen, R. Gommers, T. E. Oliphant, M. Haberland, T. Reddy, D. Cournapeau, E. Burovski, P. Peterson, W. Weckesser, J. Bright, S. J. van der Walt, M. Brett, J. Wilson, K. J. Millman, N. Mayorov, A. R. J. Nelson, E. Jones, R. Kern, E. Larson, C. J. Carey, Í. Polat, Y. Feng, E. W. Moore, J. VanderPlas, D. Laxalde, J. Perktold, R. Cimrman, I. Henriksen, E. A. Quintero, C. R. Harris, A. M. Archibald, A. H. Ribeiro, F. Pedregosa, P. van Mulbregt, and SciPy 1.0 Contributors. SciPy 1.0: Fundamental Algorithms for Scientific Computing in Python. *Nature Methods*, 17:261–272, 2020. doi: 10.1038/s41592-019-0686-2.
- [34] N. Vyas, D. Morwani, R. Zhao, I. Shapira, D. Brandfonbrener, L. Janson, and S. Kakade. SOAP: Improving and stabilizing Shampoo using Adam. *arXiv preprint arXiv:2409.11321*, 2024.
- [35] R. Ward, X. Wu, and L. Bottou. Adagrad stepsizes: Sharp convergence over nonconvex landscapes. *Journal of Machine Learning Research*, 21(219):1–30, 2020.
- [36] H. Xiao, K. Rasul, and R. Vollgraf. Fashion-mnist: a novel image dataset for benchmarking machine learning algorithms. *arXiv preprint arXiv:1708.07747*, 2017.
- [37] S. Xie, M. A. Mohamadi, and Z. Li. Adam Exploits ℓ_∞ -geometry of Loss Landscape via Coordinate-wise Adaptivity, 2024. URL <https://arxiv.org/abs/2410.08198>.
- [38] M. D. Zeiler. Adadelata: An adaptive learning rate method, 2012. URL <https://arxiv.org/abs/1212.5701>.
- [39] Y. Zhang, C. Chen, T. Ding, Z. Li, R. Sun, and Z.-Q. Luo. Why transformers need Adam: A Hessian perspective. *arXiv preprint arXiv:2402.16788*, 2024.
- [40] J. Zhao, Z. Zhang, B. Chen, Z. Wang, A. Anandkumar, and Y. Tian. Galore: Memory-efficient llm training by gradient low-rank projection. *arXiv preprint arXiv:2403.03507*, 2024.
- [41] L. Zhu, C. Liu, A. Radhakrishnan, and M. Belkin. Catapults in SGD: spikes in the training loss and their impact on generalization through feature learning. *arXiv preprint arXiv:2306.04815*, 2023.

A Deferred Proofs

Notation for proofs Throughout this section, we denote the unit sphere in d dimensions by \mathbb{S}^{d-1} and the Euclidean ball of radius r centered at \bar{x} by $\mathcal{B}(\bar{x}; r)$. Given a matrix $A \in \mathbb{R}^{m \times d}$, we write $\|A\|_F := \sqrt{\langle A, A \rangle}$ for its *Frobenius* norm and $\|A\|_{\text{op}} = \sup_{x \in \mathbb{S}^{d-1}} \|Ax\|$ for its *spectral* norm. For matrices $A, B \in \mathbb{R}^{d \times d}$, we denote the Löwner ordering by $A \preceq B$. We write $A \lesssim B$ to indicate the existence of a dimension-independent positive constant $c > 0$ such that $A \leq cB$. We write $\mathcal{O}(d, r) := \{X \in \mathbb{R}^{d \times r} \mid X^\top X = I_r\}$ and $\mathcal{O}(d) \equiv \mathcal{O}(d, d)$ for the set of matrices with orthogonal columns.

We write $\langle X, Y \rangle \stackrel{\text{def}}{=} \text{tr}(X^\top Y)$ for the Euclidean inner product and $\|X\| = \sqrt{\langle X, X \rangle}$ for its induced norm. Given a PSD matrix H we write $\langle X, Y \rangle_H$ for the weighted inner product $\langle HX, Y \rangle = \langle H^{1/2}X, H^{1/2}Y \rangle$. We write $\mathcal{O}(d)$ for the set of matrices with orthogonal columns. Given a set of scalars $\{L_i\}_{i=1}^d$, we let $\text{diag}(L_1, \dots, L_d)$ denote the $d \times d$ diagonal matrix with values L_1, \dots, L_d along the diagonal. We let $\text{mat}(\theta) \in \mathbb{R}^{m \times n}$ denote the reshaping of θ into a matrix for some m and n such that $mn = d$, and similarly we let \vec{M} denote the reshaping of a matrix into a vector.

Recall the definition of coordinate-wise smoothness constants in Eq. (1). If there exist constants $\{L_i\}_{i=1}^d$ such that $f(\cdot)$ satisfies Eq. (1) for all $\theta \in \Theta \subseteq \mathbb{R}^d$ with respect to $\{L_i\}_{i=1}^d$, then we will refer to these $\{L_i\}_{i=1}^d$ as coordinate-wise smoothness constants of $f(\cdot)$ *within domain* Θ .

A.1 Proofs from Section 3

A.1.1 Proof of Theorem 3

For convenience, we recall the definition of coordinate-wise smoothness (Eq. (1)). A function f satisfies is coordinate-wise smooth with respect to constants $L_1, \dots, L_d > 0$ if $\forall \theta_1, \theta_2 \in \mathbb{R}^d$,

$$|f(\theta_1) - f(\theta_2) - \langle \nabla f(\theta_2), \theta_1 - \theta_2 \rangle| \leq \frac{1}{2} \sum_{i=1}^d L_i (\theta_1(i) - \theta_2(i))^2.$$

We note that this is a stronger definition than the notion of coordinate-wise smoothness employed elsewhere in literature, including e.g. the analysis of randomized coordinate descent. There, the smoothness constant of the i th coordinate is defined as L'_i satisfying

$$|f(\theta + he_i) - f(\theta) + h \nabla f(\theta)(i)| \leq \frac{1}{2} h^2 L'_i.$$

Namely, this notion only considers perturbations to θ along the i th coordinate, where as the definition in Eq. 1 allows simultaneous perturbations along many coordinates.

Jiang et al. [18] and Liu et al. [22] establish upper bounds on the convergence rate of Adagrad in terms of the sum

$$L_f \stackrel{\text{def}}{=} \sum_{i=1}^d L_i$$

For example, in the case of noiseless gradients they show that the iterates $\{\theta_t\}_{t=1}^T$ produced by Adagrad satisfy

$$\frac{1}{T} \sum_{t=1}^T \|\nabla f(\theta_t)\|_1 = O\left(\frac{f(\theta^*) - f(\theta_0)}{\eta \sqrt{T}} + \frac{\eta L_f}{\sqrt{T}} \cdot \log(p(T, L_f, \nabla f(\theta_0)))\right). \quad (8)$$

where $p(T, L_f, \nabla f(\theta_0))$ is polynomial in T , L_f , and $\|\nabla f(\theta_0)\|_\infty$. In order to prove Theorem 3, we establish that for a class of non-convex functions, the sum of the coordinate-wise smoothness constants reduces significantly under reparameterization by the EGOP eigenbasis. For a function $f : \mathbb{R}^d \rightarrow \mathbb{R}$, denote by V the eigenbasis of EGOP(f) and by $\lambda_1, \dots, \lambda_d$ the eigenvalues of EGOP(f), indexed in decreasing order.

We begin with a formal statement of the result in Thm. 3.

Theorem 4. Consider a function $f : \mathbb{R}^d \rightarrow \mathbb{R}$ and a sampling distribution ρ satisfying Assumptions 1 and 2. Let $\Delta_f \stackrel{\text{def}}{=} \inf_{\theta \in \mathbb{R}^d} f(\theta) - f(\theta_0)$ for some initialization point θ_0 , and assume Δ_f is finite. Let $\{\tilde{\theta}_t\}_{t=1}^T$ denote the iterates produced by optimizing the reparameterizing objective $\tilde{f} \stackrel{\text{def}}{=} f \circ V$ using Adagrad initialized

at $V^T \theta_0$, where V denotes the eigenbasis of $\text{EGOP}(f)$. Let θ^* denote the local minimum considered in Assumption 1, and denote

$$M_p \stackrel{\text{def}}{=} \mathbb{E}_{\theta \sim \rho} [\|\theta - \theta^*\|_2^p].$$

Denote by v_1 the leading eigenvector of $\text{EGOP}(f)$, and let $\beta \stackrel{\text{def}}{=} \|v_1\|_1^2/d$. Then for any $\delta \in (0, 1)$, $\varepsilon > 0$, if the Lipschitz constant of the Hessian satisfies $H \leq \min(T_1(\delta, \varepsilon), T_2(\delta, \varepsilon))$ defined as

$$T_1 = \frac{\varepsilon \lambda_{\max}(\nabla^2 f(\theta^*))(\beta - \delta)}{2(\max_t \{\|\tilde{\theta}_t\|_2 + c\})(1 + \delta)}$$

$$T_2 = \frac{\lambda_{\max}(\nabla^2 f(\theta^*))}{M_4 \sqrt{d}} \left(\sqrt{M_3^2 + \zeta c^2 M_4} - M_3 \right)$$

where $\zeta \stackrel{\text{def}}{=} \delta/(1 + \delta)$ is sufficiently small, i.e.

$$\zeta \leq \frac{\beta \varepsilon \sqrt{1 - \varepsilon^2}}{\beta \varepsilon \sqrt{1 - \varepsilon^2} + 4 - \varepsilon^2}$$

then the convergence of reparameterized Adagrad is bounded by

$$\frac{1}{T} \sum_{t=1}^T \left\| \nabla \tilde{f}(\tilde{\theta}_t) \right\|_1 = \tilde{O} \left(\frac{\eta}{\sqrt{T}} \left(\frac{1}{\beta - \delta} \cdot \frac{\text{sr}_f}{d} \cdot L_f + \varepsilon \right) + \frac{\Delta_f}{\eta \sqrt{T}} \right).$$

Thm. 4 follows from combining the following result with the convergence guarantee in Eq. 8.

Theorem 5. Consider $f(\cdot)$ satisfying Assumptions 1 and 2. Consider the ball in \mathbb{R}^d of radius B centered at the origin. Denote by v_1 the leading eigenvector of $\text{EGOP}(f)$, and let $\beta \stackrel{\text{def}}{=} \|v_1\|_1^2/d$. Then for any $\delta \in (0, 1)$, $\varepsilon > 0$, if the Lipschitz constant of the Hessian satisfies $H \leq \min(T_1(\delta, \varepsilon), T_2(\delta, \varepsilon))$ defined as

$$T_1 = \frac{\varepsilon \lambda_{\max}(\nabla^2 f(\theta^*))(\beta - \delta)}{2(B + c)(1 + \delta)}$$

$$T_2 = \frac{\lambda_{\max}(\nabla^2 f(\theta^*))}{M_4 \sqrt{d}} \left(\sqrt{M_3^2 + \zeta c^2 M_4} - M_3 \right),$$

where $\zeta \stackrel{\text{def}}{=} \delta/(1 + \delta)$ is sufficiently small, i.e.

$$\zeta \leq \frac{\beta \varepsilon \sqrt{1 - \varepsilon^2}}{\beta \varepsilon \sqrt{1 - \varepsilon^2} + 4 - \varepsilon^2}$$

then within the ball of radius B , $f(\cdot)$ and $\tilde{f}(\cdot)$ satisfy Eq. (1) with respect to coordinate-wise smoothness constants whose sums L_f and $L_{\tilde{f}}$ respectively satisfy

$$\frac{L_{\tilde{f}}}{L_f} \leq \frac{2\sqrt{1 + \delta} \text{sr}_f}{(\beta - \delta) d} + 2\varepsilon$$

where sr_f is the stable rank of $\text{EGOP}(f)$, defined in Eq. (3).

We prove Theorem 5 by establishing the following pair of claims. The first lower bounds the term L_f :

Lemma 6. Consider $f(\cdot)$ satisfying Assumptions 1 and 2 and consider the set of dense unit vectors $\nu \in \{\pm d^{-1/2}\}^d$, the collection of vectors whose entries all have magnitude $|\nu(i)| = d^{1/2}$. Then the smoothness constants of f satisfy

$$L_f \geq \frac{d}{2c} \cdot \max_{\nu \in \{\pm d^{-1/2}\}^d} \frac{\langle \nu, \text{EGOP} \nu \rangle - \gamma}{\sqrt{\lambda_{\max}(\text{EGOP}) + \gamma}}$$

where

$$\gamma \stackrel{\text{def}}{=} 2\sqrt{d} H \lambda_{\max}(\nabla^2 f(\theta^*)) M_3 + d H^2 M_4$$

where H is the Lipschitz constant of the Hessian of $f(\cdot)$ in Assumption 2 and $M_p \stackrel{\text{def}}{=} \mathbb{E}_{\theta \sim \rho} [\|\theta - \theta^*\|_2^p]$.

If the EGOP has dense leading eigenvectors, then the term $\langle \nu, \text{EGOP } \nu \rangle$ is large. In particular, Theorem 6 implies the following:

Corollary 7. *For $f(\cdot)$ satisfying Assumptions 1 and 2, the smoothness constants of f satisfy*

$$L_f \geq \frac{d}{2c} \frac{\beta_k \lambda_k(\text{EGOP}) - \gamma}{\sqrt{\lambda_{\max}(\text{EGOP}) + \gamma}}.$$

where $\beta_k \stackrel{\text{def}}{=} \|v_k\|_1^2 / d$ for $\lambda_k(\text{EGOP}), v_k$ the k^{th} eigenvalue and eigenvector of $\text{EGOP}(f)$.

In contrast, we show that under reparameterization by the EGOP eigenbasis, the smoothness constants can be upper bounded by the following:

Lemma 8. *Let V be the eigenbasis of the EGOP of $f(\cdot)$ with respect to ρ , and define $\tilde{f}(\tilde{\theta}) \stackrel{\text{def}}{=} f(V\theta)$. Let the function $f(\cdot)$ satisfy Assumptions 1, and 2. Then within the ball of radius B centered at the origin, $\tilde{f}(\cdot)$ satisfies Eq. 1 with respect to smoothness coordinates whose sum is bounded by*

$$L_{\tilde{f}} \leq d \left(\frac{\sqrt{\gamma}}{c} + H(B + c) \right) + \frac{1}{c} \sum_{i=1}^d \sqrt{\lambda_i}$$

where γ has the same value as in Claim 7 and λ_i denotes the i th eigenvalue of the EGOP of f with respect to ρ .

Note that as Lipschitz constant of Hessian in Assumption 2 goes to zero, so does the value of γ in both Claim 7 and 8.

Theorem 5 follows from Lemmas 7 and 8. In order to prove these lemmas, we first note some consequences of Assumption 2 and establish some helper lemmas.

Helper Lemmas In order to prove Claims 7 and 8, we establish the following intermediary results. The first lemma shows that Assumption 2 implies the following bounds on the Hessian and third-derivatives of $f(\cdot)$:

Lemma 9. *Given $f(\cdot)$ satisfying Assumption 2, it follows that for all $\theta, v \in \mathbb{R}^d$,*

$$\|\nabla^3 f(\theta)[v, v]\|_{\text{op}} \leq H\sqrt{d} \|v\|^2$$

where $\nabla^3 f(\theta)[v, v]$ denotes the action of the third-derivative tensor at θ on two copies of the vector v . Also, for any $\forall v, \theta_1, \theta_2 \in \mathbb{R}^d$, $f(\cdot)$ satisfies

$$|\langle v, \nabla^2 f(\theta_1)v \rangle| \leq \langle v, \nabla^2 f(\theta_2) \rangle + H \|\theta_1 - \theta_2\|_2 \|v\|_2^2.$$

Proof. By definition, the third derivative tensor $\nabla^3 f(\theta)[v, v]$ satisfies

$$\|\nabla^3 f(\theta)[v, v]\|_2^2 = \sum_{i=1}^d \left(\sum_{j,k=1}^d v_j v_k \frac{\partial^3 f(\theta)}{\partial \theta_i \partial \theta_j \partial \theta_k} \right)^2 = \sum_{i=1}^d \left(\langle v, \left(\frac{\partial}{\partial \theta_i} \nabla^2 f(\theta) \right) v \rangle \right)^2$$

By the limit definition of the derivative,

$$\left| \langle v, \left(\frac{\partial}{\partial \theta_i} \nabla^2 f(\theta) \right) v \rangle \right| \leq \left\| \lim_{h \rightarrow 0} \frac{\nabla^2 f(\theta + h e_i) - \nabla^2 f(\theta)}{h} \right\|_{\text{op}} \|v\|^2$$

Assumption 2 implies

$$\left\| \lim_{h \rightarrow 0} \frac{\nabla^2 f(\theta + h e_i) - \nabla^2 f(\theta)}{h} \right\|_2 \leq \lim_{h \rightarrow 0} \frac{\|\nabla^2 f(\theta + h e_i) - \nabla^2 f(\theta)\|_2}{|h|} \leq H$$

We can thus bound the action of the third-derivative tensor as

$$\|\nabla^3 f(\theta)[v, v]\|_2^2 = \sum_{i=1}^d \left(\langle v, \left(\frac{\partial}{\partial \theta_i} \nabla^2 f(\theta) \right) v \rangle \right)^2 \leq \sum_{i=1}^d \left(H \|v\|_2^2 \right)^2 = H^2 d \|v\|_2^4$$

which yields the first part of the lemma.

For the second result, we note that Assumption 2 implies that $\forall v, \theta_1, \theta_2 \in \mathbb{R}^d$,

$$|\langle v, (\nabla^2 f(\theta_1) - \nabla^2 f(\theta_2)) v \rangle| \leq \|\nabla^2 f(\theta_1) - \nabla^2 f(\theta_2)\|_2 \|v\|_2^2 \leq H \|\theta_1 - \theta_2\|_2 \|v\|_2^2.$$

Thus

$$|\langle v, \nabla^2 f(\theta_1) v \rangle| - |\langle v, \nabla^2 f(\theta_2) v \rangle| \leq |\langle v, (\nabla^2 f(\theta_1) - \nabla^2 f(\theta_2)) v \rangle| \leq H \|\theta_1 - \theta_2\|_2 \|v\|_2^2$$

and re-arranging the last line yields the stated bound. \square

The second lemma gives an alternative characterization of the coordinate wise smoothness constants defined in Eq. 1. Throughout the proofs presented in this section, will use the following notation: given constants L_1, \dots, L_d , we denote by $\text{diag}(L)$ the $d \times d$ diagonal matrix with values L_1, \dots, L_d along the diagonal.

Lemma 10. *A twice-differentiable function $f : \mathbb{R}^d \rightarrow \mathbb{R}$ satisfies Eq. 1 with respect to smoothness constants L_1, \dots, L_d if and only if $\forall \theta \in \mathbb{R}^d, \forall v \in \mathbb{R}^d$,*

$$|\langle v, \nabla^2 f(\theta) v \rangle| \leq \langle v, \text{diag}(L) v \rangle$$

where $\text{diag}(L) \in \mathbb{R}^{d \times d}$ is the diagonal matrix with diagonal entries L_i .

Proof of Lemma 10. By definition, f is twice-differentiable if and only if satisfies

$$f(y) = f(x) + \langle \nabla f(x), y - x \rangle + \langle y - x, \nabla^2 f(x)(y - x) \rangle + o(\|y - x\|^2), \quad \text{for all } x, y \in \mathbb{R}^d. \quad (9)$$

We first prove the ‘‘if’’ version. By the mean value theorem,

$$\begin{aligned} f(y) - f(x) - \langle \nabla f(x), y - x \rangle &= \int_0^1 t \langle y - x, \nabla^2 f(x + t(y - x))(y - x) \rangle dt \\ &\leq \int_0^1 t \langle y - x, \text{diag}(L)(y - x) \rangle dt \\ &= \langle y - x, \text{diag}(L)(y - x) \rangle, \end{aligned}$$

where the inequality follows by assumption. Taking absolute values on both sides yields the claim.

We now prove the ‘‘only if’’ part. In particular, writing $y = x + tv$ and invoking (9), we obtain

$$\begin{aligned} |\langle y - x, \nabla^2 f(x)(y - x) \rangle| &\leq |f(y) - f(x) - \langle \nabla f(x), y - x \rangle| + o(\|y - x\|^2) \\ &\leq \langle y - x, \text{diag}(L)(y - x) \rangle + o(\|y - x\|^2) \\ &\Leftrightarrow t^2 |\langle v, \nabla^2 f(x)v \rangle| \leq t^2 \langle v, \text{diag}(L)v \rangle + o(t^2). \end{aligned}$$

Dividing both sides by t and letting $t \downarrow 0$ implies the result. \square

The third intermediate result relates the EGOP to the Hessian.

Lemma 11. *Consider thrice-differentiable function $f : \mathbb{R}^d \rightarrow \mathbb{R}$ satisfying Assumption 2, and sampling distribution ρ satisfying Assumption 1 with respect to local minimum θ^* . The EGOP of $f(\cdot)$ with respect to ρ satisfies*

$$\mathbb{E}_{\theta \sim \rho} [\nabla f(\theta) \nabla f(\theta)^\top] = H(\theta^*) + E_f(\theta^*)$$

where $H(\theta^*)$ is a PSD matrix satisfying

$$c^2 \nabla^2 f(\theta^*) \nabla^2 f(\theta^*)^\top \preceq H(\theta^*) \preceq 2c^2 \nabla^2 f(\theta^*) \nabla^2 f(\theta^*)^\top$$

and the matrix $E_f(\theta^*)$ satisfies

$$|\langle v, E_f(\theta^*)v \rangle| \leq \left(2\sqrt{d}H\lambda_{\max}(\nabla^2 f(\theta^*))M_3 + dH^2M_4 \right) \|v\|_2^2$$

where

$$M_p \stackrel{\text{def}}{=} \mathbb{E}_{\theta \sim \rho} [\|\theta - \theta^*\|_2^p].$$

Proof of Lemma 11. Given $f(\cdot)$ thrice-differentiable, the gradient $\nabla f : \mathbb{R}^d \rightarrow \mathbb{R}^d$ is a twice differentiable map. Thus applying Taylor's theorem to the gradient map implies that for any point θ there exists $\xi \in \mathbb{R}^d$ with entries $\xi_i = \alpha_i \theta_i + (1 - \alpha_i) \theta_i^*$ for some $\alpha_i \in [0, 1]$ such that

$$\nabla f(\theta) = \nabla f(\theta^*) + \nabla^2 f(\theta^*)(\theta - \theta^*) + \frac{1}{2} \nabla^3 f(\xi)[\theta - \theta^*, \theta - \theta^*]$$

where $\nabla^3 f(\xi)[\cdot, \cdot]$ denotes the action of the derivative of third-derivatives of $f(\cdot)$: for any $v \in \mathbb{R}^d$, the vector $\nabla^3 f(\xi)[v, v] \in \mathbb{R}^d$ has entries

$$(\nabla^3 f(\xi)[v, v])_i \stackrel{\text{def}}{=} \sum_{j=1}^d v_j \sum_{k=1}^d v_k \cdot \frac{\partial^3 f}{\partial \theta_i \partial \theta_j \partial \theta_k} \Big|_{\theta=\xi}.$$

For ease of notation, we let $R_f(\theta) \in \mathbb{R}^d$ denote the vector $R_f(\theta) \stackrel{\text{def}}{=} \frac{1}{2} \nabla^3 f(\xi)[\theta - \theta^*, \theta - \theta^*]$ satisfying

$$\nabla f(\theta) = \nabla f(\theta^*) + \nabla^2 f(\theta^*)(\theta - \theta^*) + R_f(\theta).$$

Given θ^* a stationary point of $f(\cdot)$, $\nabla f(\theta^*) = 0$, so the above simplifies to

$$\nabla f(\theta) = \nabla^2 f(\theta^*)(\theta - \theta^*) + R_f(\theta).$$

We can substitute the above expression into the definition of the EGOP matrix:

$$\begin{aligned} \mathbb{E}_{\theta \sim \rho} [\nabla f(\theta) \nabla f(\theta)^\top] &= \mathbb{E}_{\theta \sim \rho} \left[(\nabla^2 f(\theta^*)(\theta - \theta^*) + R_f(\theta)) (\nabla^2 f(\theta^*)(\theta - \theta^*) + R_f(\theta))^\top \right] \\ &= \mathbb{E}_{\theta \sim \rho} \left[\nabla^2 f(\theta^*)(\theta - \theta^*)(\theta - \theta^*)^\top \nabla^2 f(\theta^*)^\top \right] + E_f(\theta^*) \end{aligned}$$

where

$$E_f(\theta^*) \stackrel{\text{def}}{=} \mathbb{E}_{\theta \sim \rho} [R_f(\theta)(\theta - \theta^*)^\top \nabla^2 f(\theta^*)^\top + \nabla^2 f(\theta^*)(\theta - \theta^*)R_f(\theta)^\top + R_f(\theta)R_f(\theta)^\top].$$

We can simplify the first term by leveraging Assumption 1:

$$\begin{aligned} \mathbb{E}_{\theta \sim \rho} \left[\nabla^2 f(\theta^*)(\theta - \theta^*)(\theta - \theta^*)^\top \nabla^2 f(\theta^*)^\top \right] &= \nabla^2 f(\theta^*) \mathbb{E}_{\theta \sim \rho} [(\theta - \theta^*)(\theta - \theta^*)^\top] \nabla^2 f(\theta^*)^\top \\ &= \nabla^2 f(\theta^*) \mathbb{E}_{\theta \sim \rho} [\theta\theta^\top - \theta(\theta^*)^\top - \theta^*\theta^\top + \theta^*(\theta^*)^\top] \nabla^2 f(\theta^*)^\top \\ &= \nabla^2 f(\theta^*) (\mathbb{E}_{\theta \sim \rho} [\theta\theta^\top] + \theta^*(\theta^*)^\top) \nabla^2 f(\theta^*)^\top \\ &= \nabla^2 f(\theta^*) (c^2 \mathbb{I} + \theta^*(\theta^*)^\top) \nabla^2 f(\theta^*)^\top \end{aligned}$$

where the penultimate equality follows from the assumption that ρ is mean-zero, and the last inequality follows from the assumption that ρ is isotropic. Because θ^* is a local minimum, $\nabla^2 f(\theta^*)$ is PSD, and further the rank-1 outer product $\theta^*(\theta^*)^\top$ is also PSD, so we have

$$\nabla^2 f(\theta^*) (c^2 \mathbb{I} + \theta^*(\theta^*)^\top) \nabla^2 f(\theta^*)^\top \succeq c^2 \nabla^2 f(\theta^*) \nabla^2 f(\theta^*)^\top.$$

Moreover, Assumption 1, $\|\theta^*\|_2^2 \leq c^2$, which implies

$$\theta^*(\theta^*)^\top \preceq c^2 \mathbb{I}.$$

This implies

$$\nabla^2 f(\theta^*) (c^2 \mathbb{I} + \theta^*(\theta^*)^\top) \nabla^2 f(\theta^*)^\top \preceq 2c^2 \nabla^2 f(\theta^*) \nabla^2 f(\theta^*)^\top.$$

Combining these two matrix inequalities yields the matrix inequalities for

$$H(\theta^*) \stackrel{\text{def}}{=} \nabla^2 f(\theta^*) (c^2 \mathbb{I} + \theta^* (\theta^*)^\top) \nabla^2 f(\theta^*)^\top.$$

Lastly, we bound $|\langle v, E_f(\theta^*)v \rangle|$ for $E_f(\theta^*)$ defined above. Applying triangle inequality, Jensen's inequality, and Cauchy-Schwarz, to the definition of $E_f(\theta^*)$ yields

$$\begin{aligned} |\langle v, E_f(\theta^*)v \rangle| &\leq \mathbb{E}_{\theta \sim \rho} [2|\langle v, R_f(\theta) \rangle| \cdot |\langle \theta - \theta^*, \nabla^2 f(\theta^*)v \rangle| + |\langle v, R_f(\theta) \rangle|^2] \\ &\leq \mathbb{E}_{\theta \sim \rho} [2 \|R_f(\theta)\|_2 \|\theta - \theta^*\|_2 \lambda_{\max}(\nabla^2 f(\theta^*)) \|v\|_2^2 + \|R_f(\theta)\|_2^2 \|v\|_2^2]. \end{aligned}$$

Lemma 9 establishes that under Assumption 2, $\|R_f(\theta)\|_2 \leq H\sqrt{d}\|\theta - \theta^*\|_2$. Substituting this into the above bound yields

$$|\langle v, E_f(\theta^*)v \rangle| \leq \left(2\sqrt{d}H\lambda_{\max}(\nabla^2 f(\theta^*))M_3 + dH^2M_4 \right) \|v\|_2^2$$

where

$$M_p \stackrel{\text{def}}{=} \mathbb{E}_{\theta \sim \rho} [\|\theta - \theta^*\|_2^p].$$

□

We'll also use the following basic results from linear algebra, which we prove here for completeness.

Lemma 12. *Given $A \in \mathbb{R}^{d \times d}$ a symmetric PSD matrix, for any vector $v \in \mathbb{R}^d$,*

$$\langle v, A^\top Av \rangle \leq \lambda_{\max}(A) \langle v, Av \rangle$$

where $\lambda_{\max}(A)$ denotes the largest eigenvalue of A .

Proof of Lemma 12. Since A is PSD, it admits a square root $A^{1/2}$ which is itself PSD. Consequently,

$$\langle Av, Av \rangle = \|Av\|^2 \leq \|A^{1/2}\|_{\text{op}}^2 \|A^{1/2}v\|^2 = \lambda_{\max}(A) \langle v, Av \rangle.$$

□

Lemma 13 (Order-preserving square root). *For any positive-semidefinite matrices X, Y , the following holds:*

$$X \preceq Y \implies X^{1/2} \preceq Y^{1/2}. \quad (10)$$

Proof. Since $Y - X \succeq 0$, any unit vector v satisfies

$$0 \leq \langle v, (Y - X)v \rangle = \langle v, (Y^{1/2} + X^{1/2})(Y^{1/2} - X^{1/2})v \rangle.$$

Since X, Y are PSD, their square roots are well-defined and symmetric. In particular, the matrix $Y^{1/2} - X^{1/2}$ is symmetric and, as such, has real eigenvalues. Therefore, it suffices to prove all eigenvalues of this matrix are nonnegative.

To that end, let (λ, v) be an eigenpair of $Y^{1/2} - X^{1/2}$. We have

$$0 \leq \langle (Y^{1/2} - X^{1/2})v, (Y^{1/2} + X^{1/2})v \rangle = \lambda \langle v, (Y^{1/2} + X^{1/2})v \rangle. \quad (11)$$

In particular, assume $\lambda < 0$ (since otherwise there is nothing to show). Consequently,

$$0 > \lambda = \langle v, (Y^{1/2} - X^{1/2})v \rangle \implies \langle v, X^{1/2}v \rangle > \langle v, Y^{1/2}v \rangle \geq 0,$$

where the last inequality follows from the fact that Y is PSD. In particular, this implies that $\langle v, (Y^{1/2} + X^{1/2})v \rangle > 0$; combined with (11) and the assumption $\lambda < 0$, this yields a contradiction. Therefore, $\lambda \geq 0$. Since the choice of eigenpair was arbitrary, the claim follows. □

Dense EGOP eigenvectors lead to large \mathbf{L}_f Given the above helper lemmas, we are now equipped to prove Lemma 7.

Proof of Lemma 7. By Lemma 10, the smoothness constants L_1, \dots, L_d must satisfy

$$\forall \theta, \forall v, \quad \langle v, \text{diag}(L)v \rangle \geq |\langle v, \nabla^2 f(\theta)v \rangle|.$$

where $\text{diag}(L) \in \mathbb{R}^{d \times d}$ is the diagonal matrix with entries $\text{diag}(L)_{i,i} = L_i$. In particular, consider $\theta = \theta^*$, and let $\nu \in \{\pm d^{-1/2}\}^d$ be a dense unit vector whose entries all satisfy $|\nu(i)| = d^{-1/2}$. Then the smoothness constants must satisfy

$$\langle \nu, \text{diag}(L)\nu \rangle = \frac{1}{d} \sum_{i=1}^d L_i \geq \langle \nu, \nabla^2 f(\theta^*)\nu \rangle.$$

Given θ^* a local minimum, $\nabla^2 f(\theta^*)$ is PSD. Thus by Lemma 12,

$$\langle \nu, \nabla^2 f(\theta^*)\nu \rangle \geq \frac{1}{\lambda_{\max}(\nabla^2 f(\theta^*))} \langle \nu, \nabla^2 f(\theta^*)\nabla^2 f(\theta^*)^\top \nu \rangle$$

where $\lambda_{\max}(\nabla^2 f(\theta^*))$ denotes the leading eigenvalue of $\nabla^2 f(\theta^*)$. Moreover, Lemma 11 implies

$$\langle \nu, \nabla^2 f(\theta^*)\nabla f(\theta^*)^\top \nu \rangle \geq \frac{1}{2c^2} \langle \nu, H(\theta^*)\nu \rangle = \frac{1}{2c^2} \langle \nu, (\mathbb{E}[\nabla f(\theta)\nabla f(\theta)^\top] - E_f(\theta^*))\nu \rangle.$$

$$\langle v_1, \nabla^2 f(\theta^*)\nabla f(\theta^*)^\top v_1 \rangle \geq \frac{\lambda_{\max}(\text{EGOP}) - \langle v_1, E_f(\theta^*)v_1 \rangle}{2c^2}.$$

Chaining the preceding inequalities yields

$$\langle \nu, \text{diag}(L)\nu \rangle \geq \frac{\langle \nu, \text{EGOP} \nu \rangle - \langle \nu, E_f(\theta^*)\nu \rangle}{2c^2 \lambda_{\max}(\nabla^2 f(\theta^*))}. \quad (12)$$

Given $\nabla^2 f(\theta^*)$ PSD, we have

$$\lambda_{\max}(\nabla^2 f(\theta^*)) = \sqrt{\lambda_{\max}(\nabla^2 f(\theta^*))^2} = \sqrt{\lambda_{\max}(\nabla^2 f(\theta^*)\nabla^2 f(\theta^*)^\top)}.$$

Moreover, by Lemma 11 we have the following upper bound:

$$\begin{aligned} \lambda_{\max}(\nabla^2 f(\theta^*)\nabla^2 f(\theta^*)^\top) &\leq \frac{1}{c^2} \lambda_{\max}(H(\theta^*)) \\ &= \frac{1}{c^2} \max_{v \in \mathbb{R}^d} \langle v, (\mathbb{E}[\nabla f(\theta)\nabla f(\theta)^\top] - E_f(\theta^*))v \rangle \\ &\leq \frac{1}{c^2} (\lambda_{\max}(\text{EGOP}) + \lambda_{\max}(E_f(\theta^*))). \end{aligned}$$

Combining this inequality with the preceding equation implies

$$\lambda_{\max}(\nabla^2 f(\theta^*)) \leq \frac{1}{c} \sqrt{\lambda_{\max}(\text{EGOP}) + \lambda_{\max}(E_f(\theta^*))}.$$

Substituting this inequality into Eq. 12 implies

$$\langle \nu, \text{diag}(L)\nu \rangle \geq \frac{\langle \nu, \text{EGOP} \nu \rangle - \langle \nu, E_f(\theta^*)\nu \rangle}{2c \sqrt{\lambda_{\max}(\text{EGOP}) + \lambda_{\max}(E_f(\theta^*))}}.$$

Recall that $\nu \in \{\pm d^{-1/2}\}^d$. Thus

$$\langle \nu, \text{diag}(L)\nu \rangle = \sum_{i=1}^d L_i v(i)^2 = \frac{1}{d} \sum_{i=1}^d L_i.$$

Combining this with the above inequality implies

$$\sum_{i=1}^d L_i \geq \frac{d(\langle \nu, \text{EGOP } \nu \rangle - \langle \nu, E_f(\theta^*) \nu \rangle)}{2c\sqrt{\lambda_{\max}(\text{EGOP}) + \lambda_{\max}(E_f(\theta^*))}}.$$

By Assumption 2, $\forall v \in \mathbb{R}^d$ it holds that

$$|\langle v, E_f(\theta^*) v \rangle| \leq \gamma \|v\|_2^2$$

where

$$\gamma \stackrel{\text{def}}{=} 2\sqrt{d}H\lambda_{\max}(\nabla^2 f(\theta^*))M_3 + dH^2M_4$$

Thus

$$\sum_{i=1}^d L_i \geq \frac{d}{2c} \frac{\langle \nu, \text{EGOP } \nu \rangle - \gamma}{\sqrt{\lambda_{\max}(\text{EGOP}) + \gamma}}.$$

As this holds for all $\nu \in \{\pm d^{-1/2}\}^d$, we conclude

$$\sum_{i=1}^d L_i \geq \frac{d}{2c} \cdot \max_{\nu \in \{\pm d^{-1/2}\}^d} \frac{\langle \nu, \text{EGOP } \nu \rangle - \gamma}{\sqrt{\lambda_{\max}(\text{EGOP}) + \gamma}}.$$

We observe that for any $v \in \mathbb{R}^d$,

$$\langle v, \text{EGOP } v \rangle = \sum_{i=1}^d \lambda_i \langle v, v_i \rangle^2 \geq \max_k \lambda_k \langle v, v_k \rangle^2$$

where (λ_i, v_i) denote the i^{th} eigenvalue and eigenvector of the EGOP indexed in decreasing order of magnitude.

In particular, for any v_k , consider $\nu_k \in \mathbb{R}^d$ defined to have entries $\nu_k(i) = \text{sign}(v_k(i))d^{-1/2}$. Observe that

$$\nu_k \in \text{argmax}\{\langle \nu, v_k \rangle^2 \mid \nu \in \{\pm d^{-1/2}\}^d\}.$$

For this ν_k ,

$$\langle \nu, v_k \rangle^2 = \left(\sum_{i=1}^d \text{sign}(v_k(i))d^{-1/2}v_k(i) \right)^2 = \frac{1}{d} \left(\sum_{i=1}^d |v_k(i)| \right)^2 = \frac{1}{d} \|v_k\|_1^2.$$

Thus in general,

$$\max_{\nu \in \{\pm d^{-1/2}\}^d} \langle \nu, \text{EGOP } \nu \rangle = \max_{\nu \in \{\pm d^{-1/2}\}^d} \sum_{k=1}^d \lambda_k \langle \nu, v_k \rangle^2 \geq \max_k \frac{\lambda_k}{d} \|v_k\|_1^2.$$

This implies the lower bound

$$\sum_{i=1}^d L_i \geq \frac{d}{2c} \cdot \max_k \frac{\lambda_k \|v_k\|_1^2 / d - \gamma}{\sqrt{\lambda_{\max}(\text{EGOP}) + \gamma}}.$$

When interpreting the above inequality, we note that as the k^{th} eigenvector becomes dense, $\|v_k\|_1^2 / d \rightarrow 1$. In particular, if $v_1 \in \{\pm d^{-1/2}\}^d$, then $\|v_1\|_1^2 = (d^{-1/2} \cdot d)^2 = d$ and thus $\max_{\nu \in \{\pm d^{-1/2}\}^d} \langle \nu, v_1 \rangle^2 = 1$. Thus under this assumption, the lower bound can be simplified to

$$\sum_{i=1}^d L_i \geq \frac{d}{2c} \cdot \frac{\lambda_{\max}(\text{EGOP}) - \gamma}{\sqrt{\lambda_{\max}(\text{EGOP}) + \gamma}}.$$

□

Reparameterization by EGOP eigenbasis produces small $L_{\tilde{f}}$ In order to prove Lemma 8, we first establish the equivariance of the EGOP matrix:

Lemma 14. *For isotropic sampling distribution ρ , the EGOP matrix with respect to ρ is equivariant under reparameterization by an orthonormal matrix: for $\tilde{f}(\theta) \stackrel{\text{def}}{=} f(V\theta)$,*

$$\mathbb{E}_{\theta \sim \rho}[\nabla \tilde{f}(\theta) \nabla \tilde{f}(\theta)^\top] = V^\top \mathbb{E}_{\theta \sim \rho}[\nabla f(\theta) \nabla f(\theta)^\top] V$$

Proof. By the chain rule,

$$\nabla \tilde{f}(\theta) = V^\top \nabla f(V\theta).$$

Moreover, given ρ isotropic, for any orthonormal V we have $\rho(\theta) = \rho(V\theta)$. Thus

$$\mathbb{E}_{\theta \sim \rho}[\nabla \tilde{f}(\theta) \nabla \tilde{f}(\theta)^\top] = V^\top \mathbb{E}_{\theta \sim \rho}[\nabla f(V\theta) \nabla f(V\theta)^\top] V = V^\top \mathbb{E}_{\theta \sim \rho}[\nabla f(\theta) \nabla f(\theta)^\top] V.$$

□

An immediate corollary of Lemma 14 is that reparameterizing by the EGOP eigenbasis yields a diagonalized EGOP:

Corollary 15. *Given $f(\cdot)$ whose EGOP with respect to isometric distribution ρ has eigenvalue decomposition*

$$\mathbb{E}_{\theta \sim \rho}[\nabla f(\theta) \nabla f(\theta)^\top] = V \Lambda V^\top,$$

the reparameterized function $\tilde{f}(\theta) \stackrel{\text{def}}{=} f(V\theta)$ satisfies

$$\mathbb{E}_{\theta \sim \rho}[\nabla \tilde{f}(\theta) \nabla \tilde{f}(\theta)^\top] = V^\top \mathbb{E}_{\theta \sim \rho}[\nabla f(\theta) \nabla f(\theta)^\top] V = \Lambda.$$

Using Corollary 15, we now prove Lemma 8.

Proof of Lemma 8. Given reparameterized function $\tilde{f}(\theta) \stackrel{\text{def}}{=} f(V\theta)$, Corollary 15 implies $\mathbb{E}_{\theta \sim \rho}[\nabla \tilde{f}(\theta) \nabla \tilde{f}(\theta)^\top]$ is diagonal, and its entries are given by the eigenvalues of $\text{EGOP}(f) \stackrel{\text{def}}{=} \mathbb{E}_{\theta \sim \rho}[\nabla f(\theta) \nabla f(\theta)^\top]$. As the EGOP is an expectation of PSD matrices, these eigenvalues are all non-negative, and thus

$$\mathbb{E}_{\theta \sim \rho}[\nabla \tilde{f}(\theta) \nabla \tilde{f}(\theta)^\top]_{i,i}^{1/2} = \sqrt{\lambda_i(\text{EGOP}(f))}.$$

Thus $\forall v \in \mathbb{R}^d$,

$$\langle v, \mathbb{E}_{\theta \sim \rho}[\nabla \tilde{f}(\theta) \nabla \tilde{f}(\theta)^\top]^{1/2} v \rangle = \sum_{i=1}^d v(i)^2 \sqrt{\lambda_i(\text{EGOP}(f))}.$$

Applying Lemma 11 to the function $\tilde{f}(\cdot)$ and its corresponding local minimum $V^\top \theta^*$ implies

$$c^2 \nabla^2 \tilde{f}(V\theta^*) \nabla^2 \tilde{f}(V\theta^*) \preceq H_{\tilde{f}}(\theta^*) = \mathbb{E}_{\theta \sim \rho}[\nabla \tilde{f}(\theta) \nabla \tilde{f}(\theta)^\top] - E_{\tilde{f}}(V\theta^*)$$

where $E_{\tilde{f}}(V\theta^*)$ satisfies $\forall v \in \mathbb{R}^d$, $|\langle v, E_{\tilde{f}}(\theta^*) v \rangle| \leq \gamma \|v\|_2^2$ for

$$\gamma \stackrel{\text{def}}{=} 2\sqrt{d} H \lambda_{\max}(\nabla^2 f(\theta^*)) M_3 + d H^2 M_4$$

Thus

$$\mathbb{E}_{\theta \sim \rho}[\nabla \tilde{f}(\theta) \nabla \tilde{f}(\theta)^\top] - E_{\tilde{f}}(V\theta^*) \preceq \mathbb{E}_{\theta \sim \rho}[\nabla \tilde{f}(\theta) \nabla \tilde{f}(\theta)^\top] + \gamma \mathbb{I}.$$

Chaining the above matrix inequalities implies

$$c^2 \nabla^2 \tilde{f}(V\theta^*) \nabla^2 \tilde{f}(V\theta^*) \preceq \mathbb{E}_{\theta \sim \rho}[\nabla \tilde{f}(\theta) \nabla \tilde{f}(\theta)^\top] + \gamma \mathbb{I}.$$

Recall that the PSD ordering $X \preceq Y$ implies $X^{1/2} \preceq Y^{1/2}$ (for completeness, see statement and proof in Lemma 13 below). Thus the preceding matrix inequality implies

$$\nabla^2 \tilde{f}(V^\top \theta^*) \preceq \frac{1}{c} \left(\mathbb{E}_{\theta \sim \rho}[\nabla \tilde{f}(\theta) \nabla \tilde{f}(\theta)^\top] + \gamma \mathbb{I} \right)^{1/2}$$

Since $\mathbb{E}_{\theta \sim \rho}[\nabla \tilde{f}(\theta) \nabla \tilde{f}(\theta)^\top]$ is diagonal and $\gamma \mathbb{I}$ is diagonal,

$$\left(\mathbb{E}_{\theta \sim \rho}[\nabla \tilde{f}(\theta) \nabla \tilde{f}(\theta)^\top] + \gamma \mathbb{I} \right)_{i,i}^{1/2} = \sqrt{\mathbb{E}_{\theta \sim \rho}[\nabla \tilde{f}(\theta) \nabla \tilde{f}(\theta)^\top]_{i,i} + \gamma}.$$

Thus for all $v \in \mathbb{R}^d$, we have

$$\langle v, \nabla^2 \tilde{f}(V^\top \theta^*) v \rangle \leq \frac{1}{c} \sum_{i=1}^d v(i)^2 \sqrt{\mathbb{E}_{\theta \sim \rho}[\nabla \tilde{f}(\theta) \nabla \tilde{f}(\theta)^\top]_{i,i} + \gamma}. \quad (13)$$

Lemma 9 states that under Assumption 2, $\forall \theta, v \in \mathbb{R}^d$,

$$|\langle v, \nabla^2 f(\theta) v \rangle| \leq \langle v, \nabla^2 f(\theta^*) v \rangle + H \|\theta - \theta^*\|_2 \|v\|_2^2.$$

Applying chain rule and using the fact that orthonormal transformations are bijections on \mathbb{R}^d , this implies that $\forall \theta, v \in \mathbb{R}^d$,

$$|\langle v, \nabla^2 \tilde{f}(\theta) v \rangle| \leq \langle v, \nabla^2 \tilde{f}(V\theta^*) v \rangle + H \|\theta - \theta^*\|_2 \|v\|_2^2.$$

Combining this with the inequality in Eq. 13 implies that $\forall v \in \mathbb{R}^d$,

$$|\langle v, \nabla^2 \tilde{f}(\theta) v \rangle| \leq \sum_{i=1}^d v(i)^2 \left(\frac{1}{c} \sqrt{\mathbb{E}_{\theta \sim \rho}[\nabla \tilde{f}(\theta) \nabla \tilde{f}(\theta)^\top]_{i,i} + \gamma} + H \|\theta - \theta^*\|_2 \right).$$

Moreover, Lemma 14 implies

$$\mathbb{E}_{\theta \sim \rho}[\nabla \tilde{f}(\theta) \nabla \tilde{f}(\theta)^\top]_{i,i} = \lambda_i(\text{EGOP}(f)).$$

Thus by Lemma 10, this implies that in a ball of radius B centered at the origin, $\tilde{f}(\cdot)$ satisfies coordinate-wise smoothness with respect to constants

$$L_i \leq \frac{1}{c} \sqrt{\lambda_i(\text{EGOP}(f)) + \gamma} + H(B + c).$$

This implies the sum of the coordinate-wise smoothness constants is bounded above as

$$\begin{aligned} L_{\tilde{f}} &\leq \sum_{i=1}^d \left(\frac{1}{c} \sqrt{\lambda_i(\text{EGOP}(f)) + \gamma} + H(B + c) \right) \\ &\leq d \left(\frac{\sqrt{\gamma}}{c} + H(B + c) \right) + \frac{1}{c} \sum_{i=1}^d \sqrt{\lambda_i(\text{EGOP}(f))}. \end{aligned}$$

□

Proof of Theorem 5 Lemmas 7 and 8 imply Theorem 5:

Proof of Theorem 5. By definition of γ , if H satisfies

$$H \leq \frac{1}{M_4 \sqrt{d}} \left(\sqrt{\lambda_{\max}(\nabla^2 f(\theta^*)) M_3^2 + \Delta M_4} - \lambda_{\max}(\nabla^2 f(\theta^*)) M_3 \right),$$

then $\gamma \leq \Delta$. Thus given H satisfying

$$H \leq \frac{\lambda_{\max}(\nabla^2 f(\theta^*))}{M_4 \sqrt{d}} \left(\sqrt{M_3^2 + \zeta c^2 M_4} - M_3 \right) \quad (14)$$

we have $\gamma \leq \zeta c^2 \lambda_{\max}(\nabla^2 f(\theta^*))$. In particular, Theorem 11 implies

$$c^2 (\lambda_{\max}(\nabla^2 f(\theta^*)))^2 - \gamma \leq \lambda_{\max}(\text{EGOP}(f)) \leq c^2 (\lambda_{\max}(\nabla^2 f(\theta^*)))^2 + \gamma.$$

Thus if H satisfies Eq. (14) for some $\zeta \in [0, 1]$, then this implies

$$(1 - \zeta)c^2 (\lambda_{\max}(\nabla^2 f(\theta^*)))^2 \leq \lambda_{\max}(\text{EGOP}(f)) \leq (1 + \zeta)c^2 (\lambda_{\max}(\nabla^2 f(\theta^*)))^2$$

and thus that $\gamma \leq \delta \lambda_{\max}(\text{EGOP}(f))$ for $\delta \stackrel{\text{def}}{=} \zeta/(1 - \zeta)$.

Recall that by Theorem 6, if $\|v_1\|_1^2/d \geq \beta$, then

$$L_f \geq \frac{d}{2c} \cdot \frac{\beta \lambda_{\max}(\text{EGOP}(f)) - \gamma}{\sqrt{\lambda_{\max}(\text{EGOP}(f)) + \gamma}}.$$

Under Eq. (14),

$$\frac{\beta \lambda_{\max}(\text{EGOP}(f)) - \gamma}{\sqrt{\lambda_{\max}(\text{EGOP}(f)) + \gamma}} \geq \frac{(\beta - \delta)}{\sqrt{1 + \delta}} \sqrt{\lambda_{\max}(\text{EGOP}(f))}.$$

Thus under Eq. (14), Theorem 6 and Theorem 8 jointly imply

$$\frac{L_{\tilde{f}}}{L_f} \leq \left(d \left(\frac{\sqrt{\gamma}}{c} + H(B + c) \right) + \frac{1}{c} \sum_{i=1}^d \sqrt{\lambda_i} \right) \left(\frac{d}{2c} \cdot \frac{(\beta - \delta)}{\sqrt{1 + \delta}} \sqrt{\lambda_{\max}(\text{EGOP}(f))} \right)^{-1} \quad (15)$$

$$= \frac{2\sqrt{1 + \delta} \text{sr}_f}{(\beta - \delta) d} + \frac{2\sqrt{\gamma(1 + \delta)}}{(\beta - \delta) \sqrt{\lambda_{\max}(\text{EGOP}(f))}} + \frac{2Hc(B + c)\sqrt{1 + \delta}}{(\beta - \delta) \sqrt{\lambda_{\max}(\text{EGOP}(f))}}. \quad (16)$$

We first simplify and bound the central term in Eq. (16). Recall that under Eq. (14), $\gamma \leq \delta \lambda_{\max}(\text{EGOP}(f))$. Thus

$$\frac{2\sqrt{\gamma(1 + \delta)}}{(\beta - \delta) \sqrt{\lambda_{\max}(\text{EGOP}(f))}} \leq \frac{2\sqrt{\delta(1 + \delta)}}{\beta - \delta}.$$

In particular, if H satisfies Eq. (14) for the value

$$\zeta \leq \frac{\beta \varepsilon \sqrt{1 - \varepsilon^2}}{\beta \varepsilon \sqrt{1 - \varepsilon^2} + 4 - \varepsilon^2}$$

then

$$\delta = \frac{\zeta}{1 - \zeta} \leq \frac{2\beta \varepsilon}{4 - \varepsilon^2} \sqrt{1 - \varepsilon^2}$$

which in turn implies

$$\frac{2\sqrt{\delta(1 + \delta)}}{\beta - \delta} \leq \varepsilon.$$

We now bound the last term in Eq. (16). Recall if H satisfies Eq. (14), then

$$\frac{c^2 (\lambda_{\max}(\nabla^2 f(\theta^*)))^2}{1 + \delta} \leq \lambda_{\max}(\text{EGOP}(f)).$$

Thus if H also satisfies

$$H \leq \frac{\varepsilon \lambda_{\max}(\nabla^2 f(\theta^*))(\beta - \delta)}{2(B + c)(1 + \delta)} \quad (17)$$

then

$$\frac{2Hc(B + c)\sqrt{1 + \delta}}{(\beta - \delta) \sqrt{\lambda_{\max}(\text{EGOP}(f))}} \leq \varepsilon.$$

Thus for H satisfying Eq. (14) and Eq. (17),

$$\frac{L_{\tilde{f}}}{L_f} \leq \frac{2\sqrt{1 + \delta} \text{sr}_f}{(\beta - \delta) d} + 2\varepsilon.$$

□

A.1.2 Lipschitz Constants of Hessians in Machine Learning

In this section, we note one family of naturally-motivated non-convex objectives satisfying Assumption 2 that arise in machine learning problems. We consider the over-parameterized matrix factorization problem: let $\theta \in \mathbb{R}^{(d_1+d_2)k}$ be parameters, whose entries can be grouped into two matrices as $\theta = (L, R)$ for $L \in \mathbb{R}^{d_1 \times k}$, $R \in \mathbb{R}^{d_2 \times k}$. We define the objective

$$f(\theta) = \|\mathcal{A}(LR^\top) - b\|_2^2 \quad (18)$$

where $b \in \mathbb{R}^m$ correspond to measurements of some matrix under map $\mathcal{A}(\cdot)$, and where $\mathcal{A} : \mathbb{R}^{d_1 \times d_2} \rightarrow \mathbb{R}^m$ denotes a map

$$\mathcal{A}(X) \stackrel{\text{def}}{=} (\langle A_1, X \rangle, \dots, \langle A_m, X \rangle) \in \mathbb{R}^m.$$

We note that one a special case of Eq. 18 is the set of objectives that arise when training a two-layer linear feed-forward network using mean-squared-error loss.

We can bound the Lipschitz constant of the Hessian of this objectives in this family:

Lemma 16. *Consider the overparameterized matrix factorization objective with a linear measurement map, as defined in Eq. 18. Let $\theta \in \mathbb{R}^{(d_1+d_2)k}$ be parameters, whose entries can be grouped into two matrices: $\theta = (L, R)$ for $L \in \mathbb{R}^{d_1 \times k}$, $R \in \mathbb{R}^{d_2 \times k}$. Consider any measurement vector $b \in \mathbb{R}^m$. Then in the ball $\|\theta\|_2 \leq B$, the objective in Eq. 18 satisfies*

$$\|\nabla^2 f(\theta_1) - \nabla^2 f(\theta_2)\|_{\text{op}} \leq 12B \left(\sum_{i=1}^m \|A_i\|_F^2 \right) \|\theta_1 - \theta_2\|_2.$$

We first characterize the quadratic form of the Hessian of Eq. 18.

Lemma 17. *For the objective $f(\cdot)$ as defined in Eq. 18, for any $\theta, v \in \mathbb{R}^{(d_1+d_2)k}$ with entries denoted $\theta = (L, R)$ and $v = (U, V)$, the Hessian quadratic form can be expressed as*

$$D^2 f(L, R)[U, V] = 2 \|\mathcal{A}(UR^\top + LV^\top)\|_2^2 + 4 \langle \mathcal{A}(LR^\top) - b, \mathcal{A}(UV^\top) \rangle.$$

Proof. We begin by deriving the gradient form using the limit definition:

$$\begin{aligned} \nabla f(L, R)[U, V] &\stackrel{\text{def}}{=} \lim_{t \rightarrow 0} \frac{1}{t} (f(L + tU, R + tV) - f(L, R)) \\ &= \lim_{t \rightarrow 0} \frac{1}{t} \left(\|\mathcal{A}((L + tU)(R + tV)^\top) - b\|_2^2 - \|\mathcal{A}(LR^\top) - b\|_2^2 \right). \end{aligned}$$

By linearity of the map $\mathcal{A}(\cdot)$,

$$\begin{aligned} \mathcal{A}((L + tU)(R + tV)^\top) &= \mathcal{A}(LR^\top + tUR^\top + tLV^\top + t^2UV^\top) \\ &= \mathcal{A}(LR^\top) + t\mathcal{A}(UR^\top + LV^\top) + t^2\mathcal{A}(UV^\top). \end{aligned}$$

Substituting this into the above limit yields

$$\nabla f(L, R)[U, V] = \lim_{t \rightarrow 0} \frac{1}{t} \left(\|\Delta + t\mathcal{A}(UR^\top + LV^\top) + t^2\mathcal{A}(UV^\top)\|_2^2 - \|\Delta\|_2^2 \right)$$

where $\Delta \stackrel{\text{def}}{=} \mathcal{A}(LR^\top) - b$. Expanding the squared norm, this yields

$$\begin{aligned} \nabla f(L, R)[U, V] &= \lim_{t \rightarrow 0} \frac{1}{t} \left(\|\Delta\|_2^2 + \|t\mathcal{A}(UR^\top + LV^\top) + t^2\mathcal{A}(UV^\top)\|_2^2 \right. \\ &\quad \left. + 2\langle \Delta, t\mathcal{A}(UR^\top + LV^\top) + t^2\mathcal{A}(UV^\top) \rangle - \|\Delta\|_2^2 \right) \\ &= \lim_{t \rightarrow 0} \frac{1}{t} \left(\|t\mathcal{A}(UR^\top + LV^\top) + t^2\mathcal{A}(UV^\top)\|_2^2 \right. \\ &\quad \left. + 2\langle \Delta, t\mathcal{A}(UR^\top + LV^\top) + t^2\mathcal{A}(UV^\top) \rangle \right) \\ &= \lim_{t \rightarrow 0} \left(t \|\mathcal{A}(UR^\top + LV^\top) + t\mathcal{A}(UV^\top)\|_2^2 + 2\langle \Delta, \mathcal{A}(UR^\top + LV^\top) + t\mathcal{A}(UV^\top) \rangle \right) \\ &= 0 + 2\langle \Delta, \mathcal{A}(UR^\top + LV^\top) \rangle + 0 \\ &= 2\langle \mathcal{A}(LR^\top) - b, \mathcal{A}(UR^\top + LV^\top) \rangle \end{aligned}$$

where the last line follows from $\Delta \stackrel{\text{def}}{=} \mathcal{A}(LR^\top) - b$. Given this expression for the gradient, we can then define the Hessian quadratic form on input $v = (U, V)$ as

$$\nabla^2 f(L, R)[U, V] \stackrel{\text{def}}{=} \lim_{t \rightarrow 0} \frac{1}{t} (\nabla f(L + tU, R + tV)[U, V] - \nabla f(L, R)[U, V]).$$

Given the above expression for the gradient, this yields

$$\begin{aligned} \nabla^2 f(L, R)[U, V] &= \lim_{t \rightarrow 0} \frac{1}{t} \left(2\langle \mathcal{A}((L + tU)(R + tV)^\top) - b, \mathcal{A}(U(R + tV)^\top + (L + tU)V^\top) \rangle \right. \\ &\quad \left. - 2\langle \Delta, \mathcal{A}(UR^\top + LV^\top) \rangle \right). \end{aligned}$$

As noted above,

$$\mathcal{A}((L + tU)(R + tV)^\top) = \mathcal{A}(LR^\top) + t\mathcal{A}(UR^\top + LV^\top) + t^2\mathcal{A}(UV^\top).$$

Substituting this in to the first term in the expression for the Hessian, and using linearity of $\mathcal{A}(\cdot)$ to simplify terms, yields

$$\begin{aligned} \nabla^2 f(L, R)[U, V] &= \lim_{t \rightarrow 0} \frac{2}{t} \left(\langle \Delta + t\mathcal{A}(UR^\top + LV^\top) + t^2\mathcal{A}(UV^\top), \mathcal{A}(UR^\top + LV^\top) + 2t\mathcal{A}(UV^\top) \rangle \right. \\ &\quad \left. - \langle \Delta, \mathcal{A}(UR^\top + LV^\top) \rangle \right) \\ &= \lim_{t \rightarrow 0} \frac{2}{t} \left(\langle \Delta, \mathcal{A}(UR^\top + LV^\top) \rangle + \langle t\mathcal{A}(UR^\top + LV^\top) + t^2\mathcal{A}(UV^\top), \mathcal{A}(UR^\top + LV^\top) \rangle \right. \\ &\quad \left. + \langle \Delta, 2t\mathcal{A}(UV^\top) \rangle + \langle t\mathcal{A}(UR^\top + LV^\top) + t^2\mathcal{A}(UV^\top), 2t\mathcal{A}(UV^\top) \rangle \right. \\ &\quad \left. - \langle \Delta, \mathcal{A}(UR^\top + LV^\top) \rangle \right) \\ &= \lim_{t \rightarrow 0} \frac{2}{t} \left(\langle t\mathcal{A}(UR^\top + LV^\top) + t^2\mathcal{A}(UV^\top), \mathcal{A}(UR^\top + LV^\top) \rangle \right. \\ &\quad \left. + \langle \Delta, 2t\mathcal{A}(UV^\top) \rangle + \langle t\mathcal{A}(UR^\top + LV^\top) + t^2\mathcal{A}(UV^\top), 2t\mathcal{A}(UV^\top) \rangle \right) \\ &= \lim_{t \rightarrow 0} \frac{2}{t} \left(t\langle \mathcal{A}(UR^\top + LV^\top) + t\mathcal{A}(UV^\top), \mathcal{A}(UR^\top + LV^\top) \rangle \right. \\ &\quad \left. + 2t\langle \Delta, \mathcal{A}(UV^\top) \rangle + 2t^2\langle \mathcal{A}(UR^\top + LV^\top) + t\mathcal{A}(UV^\top), \mathcal{A}(UV^\top) \rangle \right). \end{aligned}$$

Taking the limit as $t \rightarrow 0$,

$$\begin{aligned} \nabla^2 f(L, R)[U, V] &= 2 \left(\langle \mathcal{A}(UR^\top + LV^\top), \mathcal{A}(UR^\top + LV^\top) \rangle + 2\langle \Delta, \mathcal{A}(UV^\top) \rangle \right) \\ &= 2 \left(\|\mathcal{A}(UR^\top + LV^\top)\|_2^2 + 2\langle \mathcal{A}(LR^\top) - b, \mathcal{A}(UV^\top) \rangle \right) \\ &= 2 \|\mathcal{A}(UR^\top + LV^\top)\|_2^2 + 4\langle \mathcal{A}(LR^\top) - b, \mathcal{A}(UV^\top) \rangle \end{aligned}$$

which yields the result. \square

We can prove Lemma 16, which bounds the Lipschitz constant of the Hessian of $f(\cdot)$ as defined in Eq. 18.

Proof of Lemma 16. Given some vector $v \in \mathbb{R}^{(d_1+d_2)k}$, group the entries of the vector v into two matrices: let $v = (U, V)$ for matrices $U \in \mathbb{R}^{d_1 \times k}$, $V \in \mathbb{R}^{d_2 \times k}$. Then the quadratic form of the Hessian is

$$\langle v, \nabla^2 f(\theta)v \rangle = D^2 f(L, R)[U, V].$$

The objective $f(\cdot)$ satisfies Assumption 2 with respect to Lipschitz constant H if $\forall \theta_1, \theta_2, v \in \mathbb{R}^{(d_1+d_2)k}$,

$$|\langle v, (\nabla^2 f(\theta_1) - \nabla^2 f(\theta_2))v \rangle| \leq H \|v\|_2^2 \|\theta_1 - \theta_2\|_2.$$

For any pair $\theta_1, \theta_2 \in \mathbb{R}^{(d_1+d_2)k}$, denote the entries by $\theta_1 = (L_1, R_1)$ and $\theta_2 = (L_2, R_2)$, and for any $v \in \mathbb{R}^{(d_1+d_2)k}$, denote the entries by $v = (U, V)$ as above. Then the above inequality is equivalent to

$$|D^2 f(L_1, R_1)[U, V] - D^2 f(L_2, R_2)[U, V]| \leq H (\|U\|_{\mathbb{F}}^2 + \|V\|_{\mathbb{F}}^2) \|(L_1, R_1) - (L_2, R_2)\|_2.$$

where

$$\|(L, R)\|_2 \stackrel{\text{def}}{=} \sqrt{\|L\|_{\mathbb{F}}^2 + \|R\|_{\mathbb{F}}^2} = \|\theta\|_2.$$

By Lemma 17, for any $\theta = (L, R)$ and any $v = (U, V)$, the Hessian satisfies

$$D^2 f(L, R)[U, V] = 2 \|\mathcal{A}(UR^{\top} + LV^{\top})\|_2^2 + 4\langle \mathcal{A}(LR^{\top}) - b, \mathcal{A}(UV^{\top}) \rangle.$$

By linearity of $\mathcal{A}(\cdot)$, we can expand the squared norm:

$$\begin{aligned} D^2 f(L, R)[U, V] &= 2 \|\mathcal{A}(UR^{\top}) + \mathcal{A}(LV^{\top})\|_2^2 + 4\langle \mathcal{A}(LR^{\top}) - b, \mathcal{A}(UV^{\top}) \rangle \\ &= 2 \left(\|\mathcal{A}(LV^{\top})\|_2^2 + \|\mathcal{A}(UR^{\top})\|_2^2 \right) + 4\langle \mathcal{A}(UR^{\top}), \mathcal{A}(LV^{\top}) \rangle + 4\langle \mathcal{A}(LR^{\top}) - b, \mathcal{A}(UV^{\top}) \rangle. \end{aligned}$$

Thus

$$D^2 f(L_1, R_1)[U, V] - D^2 f(L_2, R_2)[U, V] = 2 \left(\|\mathcal{A}(L_1 V^{\top})\|_2^2 - \|\mathcal{A}(L_2 V^{\top})\|_2^2 \right) \quad (19)$$

$$+ 2 \left(\|\mathcal{A}(UR_1^{\top})\|_2^2 - \|\mathcal{A}(UR_2^{\top})\|_2^2 \right) \quad (20)$$

$$+ 4 \left(\langle \mathcal{A}(UR_1^{\top}), \mathcal{A}(L_1 V^{\top}) \rangle - \langle \mathcal{A}(UR_2^{\top}), \mathcal{A}(L_2 V^{\top}) \rangle \right) \quad (21)$$

$$+ 4 \langle \mathcal{A}(L_1 R_1^{\top}) - \mathcal{A}(L_2 R_2^{\top}), \mathcal{A}(UV^{\top}) \rangle. \quad (22)$$

We bound the magnitude of each term in sequence. For the first term in Line 19, we observe

$$\begin{aligned} \left| \|\mathcal{A}(L_1 V^{\top})\|_2^2 - \|\mathcal{A}(L_2 V^{\top})\|_2^2 \right| &= |\langle \mathcal{A}(L_1 V^{\top}) + \mathcal{A}(L_2 V^{\top}), \mathcal{A}(L_1 V^{\top}) - \mathcal{A}(L_2 V^{\top}) \rangle| \\ &= |\langle \mathcal{A}((L_1 + L_2)V^{\top}), \mathcal{A}((L_1 - L_2)V^{\top}) \rangle| \\ &\leq \|\mathcal{A}((L_1 + L_2)V^{\top})\|_2 \|\mathcal{A}((L_1 - L_2)V^{\top})\|_2. \end{aligned}$$

The operator norm of $\mathcal{A}(\cdot)$ can be bounded as

$$\|\mathcal{A}(X)\|_2^2 = \sum_{i=1}^m \langle A_i, X \rangle^2 \leq \|X\|_{\mathbb{F}}^2 \sum_{i=1}^m \|A_i\|_{\mathbb{F}}^2.$$

Thus

$$\|\mathcal{A}\|_2 \leq \left(\sum_{i=1}^m \|A_i\|_{\mathbb{F}}^2 \right)^{1/2}. \quad (23)$$

We can thus bound the term in Line 19 as

$$\begin{aligned} \left| \|\mathcal{A}(L_1 V^{\top})\|_2^2 - \|\mathcal{A}(L_2 V^{\top})\|_2^2 \right| &\leq \|\mathcal{A}((L_1 + L_2)V^{\top})\|_2 \|\mathcal{A}((L_1 - L_2)V^{\top})\|_2 \\ &\leq \|\mathcal{A}\|_2^2 \|(L_1 + L_2)V^{\top}\|_{\mathbb{F}} \|(L_1 - L_2)V^{\top}\|_{\mathbb{F}} \\ &\leq \|\mathcal{A}\|_2^2 \|L_1 + L_2\|_{\mathbb{F}} \|V\|_{\mathbb{F}} \|L_1 - L_2\|_{\mathbb{F}} \|V\|_{\mathbb{F}}. \end{aligned}$$

In the ball $\|\theta\|_2 \leq B$, we have that for $\theta = (L, R)$

$$\|L\|_{\mathbb{F}} \leq \|\theta\|_2 \leq B.$$

Thus $\|L_1 + L_2\|_{\mathbb{F}} \leq 2B$, so we can bound

$$\begin{aligned} \left| \|\mathcal{A}(L_1 V^{\top})\|_2^2 - \|\mathcal{A}(L_2 V^{\top})\|_2^2 \right| &\leq 2B \|\mathcal{A}\|_2^2 \|V\|_{\mathbb{F}}^2 \|L_1 - L_2\|_{\mathbb{F}} \\ &\leq 2B \|\mathcal{A}\|_2^2 \|V\|_{\mathbb{F}}^2 \|(L_1, R_1) - (L_2, R_2)\|_2 \end{aligned}$$

where the last line follows by

$$\|(L_1, R_1) - (L_2, R_2)\|_2 \stackrel{\text{def}}{=} \sqrt{\|L_1 - L_2\|_F^2 + \|R_1 - R_2\|_F^2} \geq \|L_1 - L_2\|_F.$$

An analogous argument bounds the term in Line 20 as

$$\left| \|\mathcal{A}(UR_1^\top)\|_2^2 - \|\mathcal{A}(UR_2^\top)\|_2^2 \right| \leq 2B \|\mathcal{A}\|_2^2 \|U\|_F^2 \|(L_1, R_1) - (L_2, R_2)\|_2.$$

To bound the term in Line 21, we first observe that

$$\begin{aligned} & \langle \mathcal{A}(UR_1^\top), \mathcal{A}(L_1V^\top) \rangle - \langle \mathcal{A}(UR_2^\top), \mathcal{A}(L_2V^\top) \rangle \\ &= \langle \mathcal{A}(UR_1^\top), \mathcal{A}(L_1V^\top) \rangle - \langle \mathcal{A}(L_1V^\top), \mathcal{A}(UR_2^\top) \rangle + \langle \mathcal{A}(L_1V^\top), \mathcal{A}(UR_2^\top) \rangle - \langle \mathcal{A}(UR_2^\top), \mathcal{A}(L_2V^\top) \rangle \\ &= \langle \mathcal{A}(UR_1^\top) - \mathcal{A}(UR_2^\top), \mathcal{A}(L_1V^\top) \rangle + \langle \mathcal{A}(L_1V^\top) - \mathcal{A}(L_2V^\top), \mathcal{A}(UR_2^\top) \rangle \\ &= \langle \mathcal{A}(U(R_1 - R_2)^\top), \mathcal{A}(L_1V^\top) \rangle + \langle \mathcal{A}((L_1 - L_2)V^\top), \mathcal{A}(UR_2^\top) \rangle \end{aligned}$$

Thus

$$\begin{aligned} & |\langle \mathcal{A}(UR_1^\top), \mathcal{A}(L_1V^\top) \rangle - \langle \mathcal{A}(UR_2^\top), \mathcal{A}(L_2V^\top) \rangle| \\ &= |\langle \mathcal{A}(U(R_1 - R_2)^\top), \mathcal{A}(L_1V^\top) \rangle + \langle \mathcal{A}((L_1 - L_2)V^\top), \mathcal{A}(UR_2^\top) \rangle| \\ &\leq \|\mathcal{A}(U(R_1 - R_2)^\top)\|_2 \|\mathcal{A}(L_1V^\top)\|_2 + \|\mathcal{A}((L_1 - L_2)V^\top)\|_2 \|\mathcal{A}(UR_2^\top)\|_2 \\ &\leq \|\mathcal{A}\|_2^2 \|U(R_1 - R_2)^\top\|_F \|L_1V^\top\|_F + \|\mathcal{A}\|_2^2 \|(L_1 - L_2)V^\top\|_F \|UR_2^\top\|_F \\ &\leq \|\mathcal{A}\|_2^2 \|U\|_F \|R_1 - R_2\|_F \|L_1\|_F \|V\|_F + \|\mathcal{A}\|_2^2 \|L_1 - L_2\|_F \|V\|_F \|U\|_F \|R_2\|_F \\ &= \|\mathcal{A}\|_2^2 \|U\|_F \|V\|_F (\|R_1 - R_2\|_F \|L_1\|_F + \|L_1 - L_2\|_F \|R_2\|_F) \end{aligned}$$

In the ball $\|\theta\|_2 \leq B$, we have that for $\|L_1\|_F \leq B$ and $\|R_2\|_F \leq B$. Thus

$$\begin{aligned} & |\langle \mathcal{A}(UR_1^\top), \mathcal{A}(L_1V^\top) \rangle - \langle \mathcal{A}(UR_2^\top), \mathcal{A}(L_2V^\top) \rangle| \\ &\leq B \|\mathcal{A}\|_2^2 \|U\|_F \|V\|_F (\|R_1 - R_2\|_F + \|L_1 - L_2\|_F). \end{aligned}$$

Recall that for any $a, b \in R$, it holds that $a + b \leq 2\sqrt{a^2 + b^2}$ and $2ab \leq a^2 + b^2$. Thus

$$\|R_1 - R_2\|_F + \|L_1 - L_2\|_F \leq 2\sqrt{\|L_1 - L_2\|_F^2 + \|R_1 - R_2\|_F^2} = 2\|(L_1, R_1) - (L_2, R_2)\|_2$$

and

$$\|U\|_F \|V\|_F \leq \frac{1}{2} (\|U\|_F^2 + \|V\|_F^2).$$

Combining these bounds yields

$$\begin{aligned} & |\langle \mathcal{A}(UR_1^\top), \mathcal{A}(L_1V^\top) \rangle - \langle \mathcal{A}(UR_2^\top), \mathcal{A}(L_2V^\top) \rangle| \\ &\leq B \|\mathcal{A}\|_2^2 (\|U\|_F^2 + \|V\|_F^2) \|(L_1, R_1) - (L_2, R_2)\|_2. \end{aligned}$$

Lastly, we bound the term in Line 22. We begin by observing that

$$\begin{aligned} \mathcal{A}(L_1R_1^\top) - \mathcal{A}(L_2R_2^\top) &= \mathcal{A}(L_1R_1^\top) - \mathcal{A}(L_1R_2^\top) + \mathcal{A}(L_1R_2^\top) - \mathcal{A}(L_2R_2^\top) \\ &= \mathcal{A}(L_1(R_1 - R_2)^\top) + \mathcal{A}((L_1 - L_2)R_2^\top) \end{aligned}$$

Thus

$$\begin{aligned} & |\langle \mathcal{A}(L_1R_1^\top) - \mathcal{A}(L_2R_2^\top), \mathcal{A}(UV^\top) \rangle| = |\langle \mathcal{A}(L_1(R_1 - R_2)^\top) + \mathcal{A}((L_1 - L_2)R_2^\top), \mathcal{A}(UV^\top) \rangle| \\ &= |\langle \mathcal{A}(L_1(R_1 - R_2)^\top), \mathcal{A}(UV^\top) \rangle + \langle \mathcal{A}((L_1 - L_2)R_2^\top), \mathcal{A}(UV^\top) \rangle| \\ &\leq \|\mathcal{A}(L_1(R_1 - R_2)^\top)\|_2 \|\mathcal{A}(UV^\top)\|_2 + \|\mathcal{A}((L_1 - L_2)R_2^\top)\|_2 \|\mathcal{A}(UV^\top)\|_2 \\ &\leq \|\mathcal{A}\|_2^2 \|L_1(R_1 - R_2)^\top\|_F \|UV^\top\|_F + \|\mathcal{A}\|_2^2 \|(L_1 - L_2)R_2^\top\|_F \|UV^\top\|_F \\ &\leq \|\mathcal{A}\|_2^2 (\|L_1\|_F \|R_1 - R_2\|_F \|U\|_F \|V\|_F + \|L_1 - L_2\|_F \|R_2\|_F \|U\|_F \|V\|_F) \\ &= \|\mathcal{A}\|_2^2 \|U\|_F \|V\|_F (\|L_1\|_F \|R_1 - R_2\|_F + \|L_1 - L_2\|_F \|R_2\|_F). \end{aligned}$$

In the ball $\|\theta\|_2 \leq B$, we have that for $\|L_1\|_F \leq B$ and $\|R_2\|_F \leq B$. Thus

$$|\langle \mathcal{A}(L_1 R_1^\top) - \mathcal{A}(L_2 R_2^\top), \mathcal{A}(UV^\top) \rangle| \leq B \|\mathcal{A}\|_2^2 \|U\|_F \|V\|_F (\|R_1 - R_2\|_F + \|L_1 - L_2\|_F).$$

Recalling the bounds $\|V\|_F \|U\|_F$ and $(\|L_1 - L_2\|_F + \|R_1 - R_2\|_F)$ established above, we have

$$|\langle \mathcal{A}(L_1 R_1^\top) - \mathcal{A}(L_2 R_2^\top), \mathcal{A}(UV^\top) \rangle| \leq B \|\mathcal{A}\|_2^2 (\|U\|_F^2 + \|V\|_F^2) \|(L_1, R_1) - (L_2, R_2)\|_2.$$

Employing triangle inequality and each of the above bounds implies

$$\begin{aligned} |D^2 f(L_1, R_1)[U, V] - D^2 f(L_2, R_2)[U, V]| &\leq 2 \cdot 2B \|\mathcal{A}\|_2^2 \|V\|_F^2 \|(L_1, R_1) - (L_2, R_2)\|_2 \\ &\quad + 2 \cdot 2B \|\mathcal{A}\|_2^2 \|U\|_F^2 \|(L_1, R_1) - (L_2, R_2)\|_2 \\ &\quad + 4B \|\mathcal{A}\|_2^2 (\|U\|_F^2 + \|V\|_F^2) \|(L_1, R_1) - (L_2, R_2)\|_2 \\ &\quad + 4B \|\mathcal{A}\|_2^2 (\|U\|_F^2 + \|V\|_F^2) \|(L_1, R_1) - (L_2, R_2)\|_2 \\ &\leq 12B \|\mathcal{A}\|_2^2 (\|U\|_F^2 + \|V\|_F^2) \|(L_1, R_1) - (L_2, R_2)\|_2 \end{aligned}$$

which implies the result. \square

A.2 Proofs from Section 4

In Section 4, we noted that for objectives of the form $f(\theta) = h(A\theta)$, for some loss function $h(\cdot)$ and data matrix $A \in \mathbb{R}^{d \times n}$, the EGOP of $f(\cdot)$ is

$$\text{EGOP}(f) = A^\top \mathbb{E}_{\theta \sim \rho} [\nabla_\theta h(A\theta) \nabla_\theta h(A\theta)^\top] A \quad (24)$$

For general loss functions $h(\cdot)$, one can establish the following upper bounds showing how the singular values of A control the EGOP eigenspectrum of $f(\cdot)$.

Lemma 18. *Consider $f : \mathbb{R}^n \rightarrow \mathbb{R}$ satisfying $f(\theta) = h(A\theta)$ for some loss function $h : \mathbb{R}^n \rightarrow \mathbb{R}$ and nonsingular data matrix $A \in \mathbb{R}^{n \times n}$. Denote by $\sigma_i(\cdot)$ and $\lambda_i(\cdot)$ the i th singular value and eigenvalue of a matrix respectively, indexed by decreasing value. Then all nonzero eigenvalues of the EGOP of $f(\cdot)$ satisfy*

$$\frac{\lambda_k(\text{EGOP}(f))}{\lambda_1(\text{EGOP}(f))} \leq \left(\frac{\sigma_k(A)}{\sigma_1(A)} \right)^2 \frac{\lambda_1(M)}{\lambda_n(M)}.$$

where

$$M \stackrel{\text{def}}{=} \mathbb{E}_{\theta \sim \rho} [\nabla_\theta h(A\theta) \nabla_\theta h(A\theta)^\top].$$

If the matrix M has some finite condition number that does not go to infinity as the spectral decay in A increases, then Lemma 18 shows that increasing spectral decay in the data matrix A induces spectral decay in the EGOP eigenvalues of $f(\cdot)$.

For specific choices of $h(\cdot)$, such as $h(\cdot) \stackrel{\text{def}}{=}} \|\cdot\|_2^2$, one can more precisely characterize how spectral decay in the matrix A induces decay in the EGOP of $f \stackrel{\text{def}}{=} h \circ A$.

Lemma 19. *Consider $A \in \mathbb{R}^{d \times n}$ and let $f(\theta) = \frac{1}{2} \|A\theta - y\|_2^2$ where $y = A\theta^* + \eta$, for η some mean-zero measurement noise. Assume sampling density ρ is a standard Gaussian distribution. Then the eigenvalues of $\text{EGOP}(f)$, $\{\lambda_k\}_{k=1}^d$ indexed in decreasing order, satisfy*

$$\frac{\lambda_k}{\lambda_1} \leq \left(\frac{\sigma_{k-1}(A)}{\sigma_1(A)} \right)^4 \quad \forall k \in [2, \dots, n] \quad (25)$$

where $\sigma_i(A)$ denotes the i^{th} singular value of A , indexed in decreasing order.

Proof. Observe that for any $\theta \in \mathbb{R}^d$,

$$\nabla f(\theta) = A^\top(A\theta - y) = A^\top(A\theta - A\theta^* - A\eta) = A^\top A(\theta - \theta^*) + A\eta.$$

Thus for ρ a standard Gaussian,

$$\begin{aligned} \text{EGOP}(f) &= \mathbb{E}_{\theta \sim \rho} \left[(A^\top(A\theta - y)) (A^\top(A\theta - y))^\top \right] \\ &= A^\top \mathbb{E}_{\theta \sim \rho} [A\theta\theta^\top A + yy^\top] A \\ &= (A^\top A)^2 + (A^\top y)(A^\top y)^\top \end{aligned}$$

using the fact that ρ is mean-zero and isotropic. Thus $\text{EGOP}(f)$ is a rank-1 perturbation of the matrix $(A^\top A)^2$, which is itself PSD and has eigenvalues $\sigma_k(A)^4$. Moreover if we let $A = Q_1 \Sigma Q_2^\top$ denote the SVD of A , we can rewrite

$$\text{EGOP}(f) = Q_2 (\Sigma^4 + \Sigma Q_1^\top yy^\top Q_1 \Sigma) V^\top$$

where Σ^4 is diagonal and has entries $\{\sigma_i^4(A)\}_{i=1}^n$. By Golub [14], the eigenvalues of $\text{EGOP}(f)$ thus satisfy

$$\sigma_i^4(A) \geq \lambda_i(\text{EGOP}(f)) \geq \sigma_{i+1}^4(A) \quad \forall i \in [2, \dots, n]$$

and

$$\sigma_1^4(A) + \|\Sigma Q_1^\top y\|_2^2 \geq \lambda_1(\text{EGOP}) \geq \sigma_2^4(A)$$

which implies the result. \square

B Expanded Discussion of Heuristics for Scalability and Efficient Implementation

In this section, we expand on the heuristics proposed in Section 5.

Sampling gradients Gradient sampling can be performed in parallel, since we assume gradients are evaluated at points drawn i.i.d. Moreover, as discussed below, we hypothesize that to obtain a benefit from EGOP reparameterization it suffices to obtain an accurate estimate of only the leading eigenvectors of the EGOP eigenmatrix. Thus for functions with strong spectral decay it suffices to use a conservative number of gradient samples ($M \lesssim d$ for M the number of samples and d the number of problem parameters).

Forming EGOP Eigenbasis For applications with large numbers of parameters, computing a full, exact eigendecomposition of the empirical EGOP matrix may pose a significant expense. However, we hypothesize that for functions with strong spectral decay it suffices to obtain accurate estimates of only the leading EGOP eigenvectors, and that use of any random orthonormal basis for the eigenspaces of smaller eigenvalues suffices. Indeed when using random sampling to empirically estimate the EGOP, the error in the estimate of the subspace of the leading k eigenvectors is proportionate to the eigengap λ_k/λ_{k+1} (for a formal statement of this result, see Corollary 3.10 in Constantine [6]). Thus when executing Algorithm 1 with a small number of gradient samples (e.g. $M \lesssim d$), one is effectively only obtaining an estimate of the leading EGOP eigenvectors. In Section 6, we include results obtained by using a small number of gradient samples ($M = d$) to estimate the EGOP, placing these empirical studies within this regime.

In light of this differential error between the leading and smaller eigenspaces, we propose that to save computational expense one can employ techniques like randomized SVD in order to form $V_k \in \mathbb{R}^{d \times k}$, a matrix whose columns contain the estimated k leading eigenvectors of the EGOP, and then use any random orthonormal basis for the orthogonal complement to form a complete $d \times d$ change-of-basis matrix.

Storing and applying change-of-basis matrix. In key applications of adaptive algorithms, particularly training neural networks, the number of problem parameters may be so large that storing and applying change-of-basis matrices on iterations becomes a nontrivial expense. In this section we consider several heuristics tailored to these applications and we note that many of the heuristics from this section—particularly the *block reparameterization* described below—also reduce the cost of sampling gradients and forming the EGOP eigenbasis.

For any objective, one can reduce the cost of maintaining and applying $V \in \mathbb{R}^{d \times d}$ by forming some sparse or factorized approximation of V . For example, consider computing a Kronecker-product approximation to V , i.e. finding matrices $V_1 \in \mathbb{R}^{m_1 \times n_1}, V_2 \in \mathbb{R}^{m_2 \times n_2}$ for $m_1 m_2 = n_1 n_2 = d$ such that $V \approx V_1 \otimes V_2$. This reduces the storage cost from d^2 to $m_1 n_1 + m_2 n_2$, which can be significantly lower depending on choice of the factorization dimensions m_i, n_i . Such a factorization is similar to the method proposed by Vyas et al. [34].

Instead of computing and retaining a full orthogonal basis $V \in \mathbb{R}^{d \times d}$, one could form a projection matrix $V \in \mathbb{R}^{d \times k}$ for some user-chosen reduced dimension k . This would require storing and applying a matrix of size $\mathbb{R}^{n_{in} n_{out} \times k}$ instead of $\mathbb{R}^{n_{in} n_{out} \times n_{in} n_{out}}$, and the k leading eigenvectors can be efficiently estimated using randomized SVD, as discussed earlier. Zhao et al. [40] studies a related method for reparameterizing adaptive methods using a partial basis, but find that it is necessary to periodically re-compute the projection in order to achieve good performance.

Block Reparameterization Here we instantiate block reparameterization for multilayer neural networks. Given an L -layer neural network whose i th layer is parameterized by weight matrix $W_i \in \mathbb{R}^{n_{in}^{(i)} \times n_{out}^{(i)}}$ and bias vector $b_i \in \mathbb{R}^{n_{out}^{(i)}}$, we consider optimizing $f(\theta) = \text{loss}(\theta; X_{\text{train}}, y_{\text{train}})$ with respect to parameters $\theta = [(W_1, b_1), \dots, (W_L, b_L)]$.

Rather than forming the full EGOP as described in Algorithm 1, we consider estimating the *layer* EGOP matrices

$$\text{EGOP}^{(i)} \stackrel{\text{def}}{=} \frac{1}{M} \sum_{k=1}^M \nabla_{W_i} f(\theta_k) \nabla_{W_i} f(\theta_k)^\top$$

where $\nabla_{W_i} f(\theta_k) \in \mathbb{R}^{n_{in}^{(i)} n_{out}^{(i)}}$ is the vector of partial derivatives of f w.r.t. the entries of W_i evaluated at θ_k , and the points $\{\theta_k\}_{k=1}^M \sim \rho$ are drawn i.i.d..

Given these L empirical layer EGOP matrices, one can obtain L change-of-basis matrices

$$V^{(i)} \in \mathbb{R}^{n_{in}^{(i)} n_{out}^{(i)} \times n_{in}^{(i)} n_{out}^{(i)}}$$

and form the objective

$$\tilde{f}(\theta) = f([(V^{(1)} W_1, b_1), \dots, (V^{(L)} W_L, b_L)]).$$

Block EGOP reparameterization requires storing and applying L orthonormal matrices, each of size $n_{in}^{(i)} n_{out}^{(i)} \times n_{in}^{(i)} n_{out}^{(i)}$. For deep neural networks, this can be considerably less expensive than storing and applying the global change-of-basis matrix, which would be of size $\sum_{i=1}^L n_{in}^{(i)} n_{out}^{(i)} \times \sum_{i=1}^L n_{in}^{(i)} n_{out}^{(i)}$. This may also reduce the sampling cost; each layer EGOP is of smaller dimension than the global EGOP and thus has a smaller number of eigenvectors to estimate. Thus the layer EGOP eigenbases may be estimated with fewer total gradient samples.

Another benefit to block EGOP reparameterization is that it offers an easy way to reduce cost by choosing to only reparameterize a subset of layers. Thus for example if a network has a subset of layers which are too wide to efficiently reparameterize, one can choose to only reparameterize the narrower layers.

For networks where the first layer involves a linear transformation of the input data, reparameterizing only the first layer corresponds to an orthogonal transformation of the data. Thus pre-computing the EGOP eigenbasis and applying this matrix to the input data up-front would allow one to reparameterize the first layer, without requiring one to store and apply the change-of-basis matrix during training.

C Supplementary Figures

C.1 Supplementary Figures for Section 4

Spectral decay is robust to choice of sampling distribution In Figure 6, we present evidence that spectral decay visualized in Figure 2 is robust to choice of sampling distribution. The EGOP whose eigenspectrum is displayed in Fig. 2 was generated from gradient samples $\nabla f(\theta_i)$ for $\theta_i \sim \mathcal{N}(0, \mathbb{I})$, but as visualized in later figures (Fig. 6), the level of spectral decay is comparable to that obtained with Gaussian distributions of differing scales. We also compare to the spectral decay exhibited by the EGOP matrix when ρ is taken to be an initialization distribution used in practice [13]. For details on this distribution, see Appendix D.5. We also note that the interesting shelf structure of the leading eigenvalues is also robust to choice of sampling distribution, as illustrated in Fig. 6. Full details for the objective and EGOP estimation procedure for this figure are detailed in Appendix D.4.

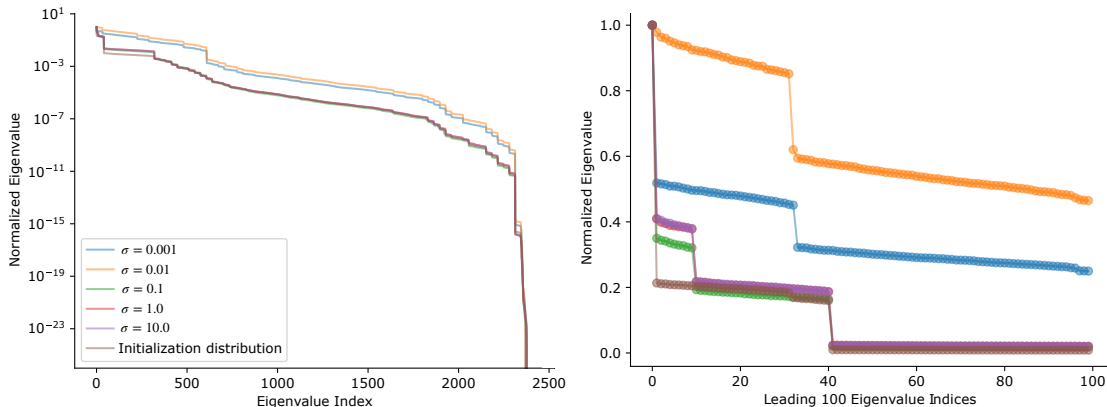


Figure 6: Comparing EGOP spectral decay of a 2-layer ReLU network on tinyMNIST dataset. Plot displays the ratio λ_k/λ_1 as a function of eigenvalue index k , for eigenvalues indexed in decreasing order. The blue, orange, green, red, and purple colored traces display the eigenspectrum of the EGOP with respect to a mean-zero Gaussian with covariance $\sigma^2\mathbb{I}$, for varying values of σ . The brown trace displays the eigenspectrum of the EGOP with respect to a realistic initialization distribution for this architecture: weights for each layer are drawn from a scaled Xavier normal distribution, and biases are initialized from a scaled uniform distribution (see Appendix D.5). We observe that under all sampling distributions, the eigenspectrum exhibits spectral decay, and that the realistic initialization distribution has spectral decay very comparable to that of the standard Gaussian, displayed in Fig. 2 in the main body.

Spectral decay persists in block EGOP matrices Fig. 7 plots the normalized eigenspectra of the block matrices corresponding to the first and second layers of ReLU networks on the UCI digits dataset and fashionMNIST dataset respectively. For full details on these datasets and the architectures used, see Appendix D.4. Interestingly, both datasets exhibit shared characteristics: the normalized spectral decay in the first layer is strikingly similar, and in both networks the spectral decay in the first layer is more pronounced than in the second layer.

Density of leading EGOP eigenvectors Theorem 3 shows that when the leading EGOP eigenvector is dense, reparameterized Adagrad enjoys much stronger convergence guarantees. Density of the k^{th} eigenvector is measured by $\beta_k \stackrel{\text{def}}{=} \|v_k\|_1^2$. Theorem 3 states a guarantee in terms of $\beta \stackrel{\text{def}}{=} \beta_1$, the density of the leading eigenvector.

In order for the leading term in Theorem 3 in the bound for reparameterized Adagrad to scale as $\tilde{O}((sr_f/d) \cdot (\eta L_f/\sqrt{T}))$, it is sufficient that $O(\beta - 1/3)^{-1} = 1$, or in particular that $\beta - 1/3 \gg 1/d$. In Fig. 8, we show that for the UCI digits dataset, this condition is satisfied. Specifically, we show that $\beta > 0.5$, while for this network $1/d < 5e - 4$, meaning that indeed $\beta - 1/3 \gg 1/d$. Moreover we show that not only

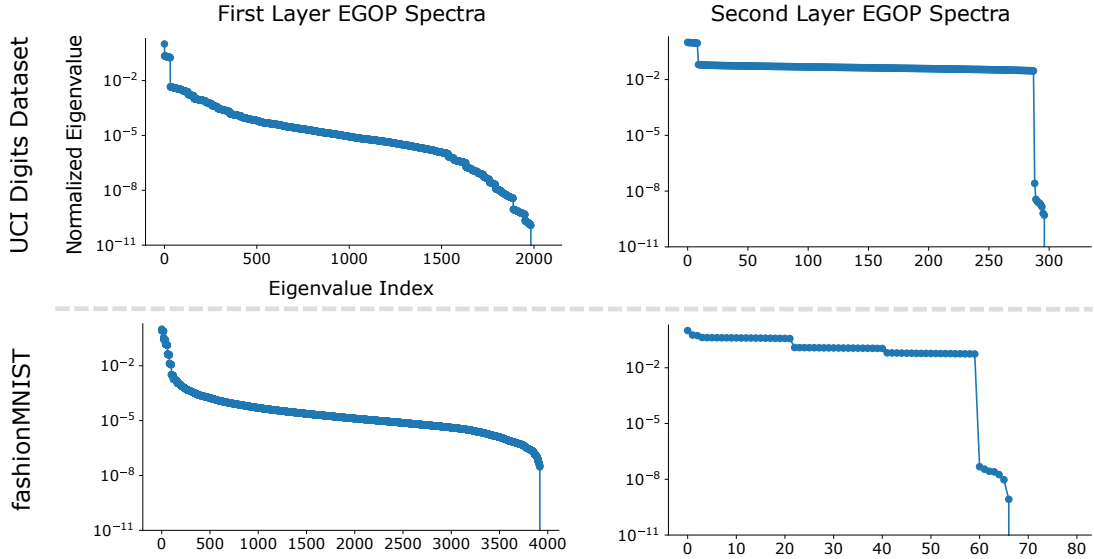


Figure 7: Eigenspectra of the layerwise EGOP matrices of neural networks on `tinyMNIST` and `fashionMNIST`. The spectral decay observed in Fig. 2 persists for layer EGOP matrices, defined in Section 5, and across datasets. Y-axes for all figures display identical ranges.

does the leading eigenvector satisfy this density assumption, but several of the leading eigenvectors satisfy $\beta_k - 1/3 \gg 1/d$.

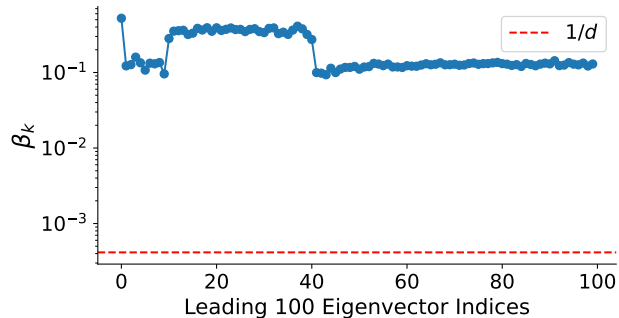
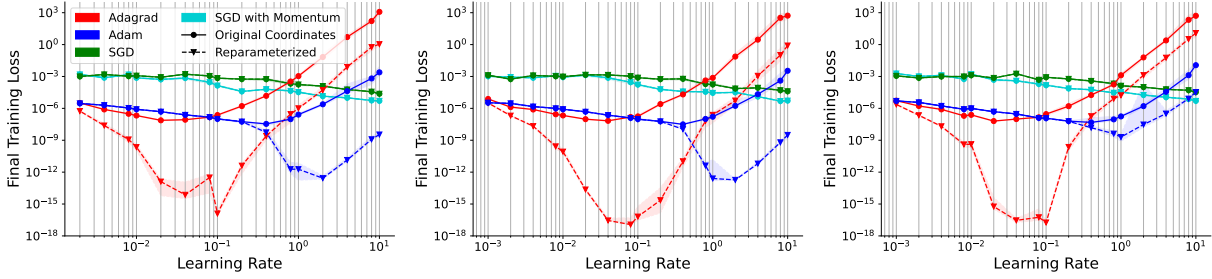


Figure 8: Plotting the density measure $\beta_k \stackrel{\text{def}}{=} \|v_k\|_1^2$ for the leading 100 eigenvectors of $\text{EGOP}(f)$, where $f(\cdot)$ is the cross-entropy loss of a 2-layer ReLU neural network on the UCI digits training dataset. The leading eigenvector satisfies $\beta > 0.5$ and several have density $\beta_k > 0.3$. We visualize the value $1/d$ in red (for this example, $d = 2,410$) to verify that for the leading eigenvectors, $\beta_k \gg 1/d$.

C.2 Supplementary Figures for Section 6

Multilayer linear networks We compare three methods for EGOP reparameterization in order to examine some heuristics proposed in Section 5. In Fig. 9, we consider training a multilayer linear network (6) under global EGOP reparameterization, wherein all parameters are reparameterized simultaneously as in Algorithm 1 (Fig. 9a); block reparameterization for all layers, following the procedure defined in Section 5 (Fig. 9b); and block reparameterization of only the parameters in the first layer (Fig. 9c). For all three methods, we estimate the EGOP using the same number of gradient samples: $M = 2d$, where d is the total number of network parameters.

Comparing Fig. 9a with Fig. 9b shows that for this problem, EGOP reparameterization offers compa-

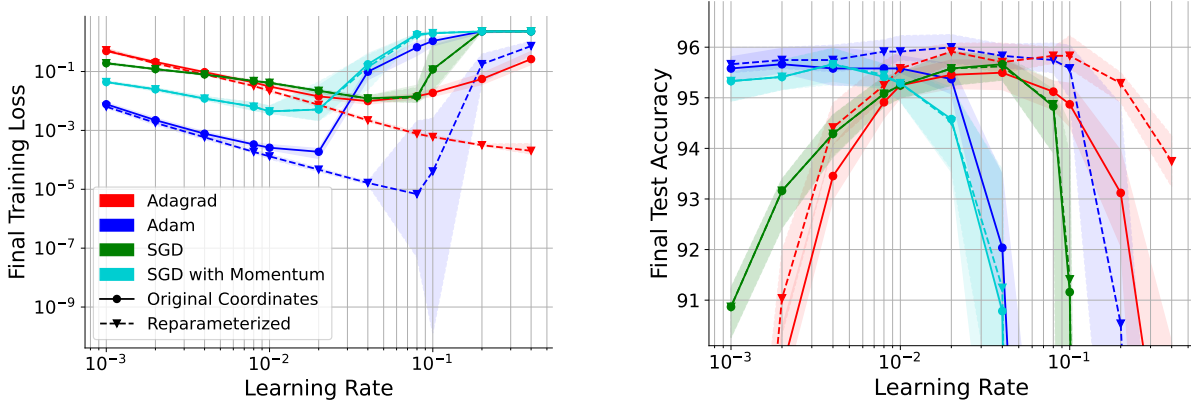


(a) Global EGOP Reparameterization (b) Block reparameterization, all layers (c) First layer only

Figure 9: Comparing three EGOP reparameterization methods for training a multilayer linear network (6). Fig. 9a is a reproduction of Fig. 3b in the main body, and shows results for performing EGOP reparameterization of all parameters simultaneously. Fig. 9b shows results when performing block EGOP reparameterization, where each network layer forms a block. Fig. 9c shows results when block-reparameterizing only the parameters in the first layer.

able benefit when using block reparameterization as when using global reparameterization. This suggests that block EGOP reparameterization, which has a reduced computational cost compared to global EGOP reparameterization, may be an effective way to accelerate adaptive methods when problem instances are too large to permit global reparameterization. Reparameterizing only the first layer (Fig. 9c) improves Adagrad’s performance by a margin comparable to that of global and block reparameterization of all layers, but the benefit to Adam under reparameterization of only the first layer is much less pronounced.

Image Classification with ReLU Networks Fig. 10 expands on the results shown in Fig. 1 (right) for 2-layer ReLU networks on the UCI digits dataset. Fig. 10a plots final training loss versus learning rate, and shows that benefit of reparameterization shown in Fig. 1 is robust to choice of learning rate. Fig. 10b plots final test accuracy versus learning rate, and shows that the improved training offered by reparameterization does not lead to over-fitting. For full experimental details on the architecture, dataset, and loss function used for these experiments, see Appendix C.2.



(a) Median final training loss versus learning rate (b) Median final test accuracy versus learning rate

Figure 10: Training loss and test accuracy results for the UCI digits dataset image classification task. Results are aggregated over independent trials corresponding to different random initializations. Medians are plotted as traces, and shaded regions indicate the 25th-75th percentiles.

Similarly, Fig. 11 expands on the results presented in Fig. 4. Fig. 11a shows that benefit of reparameterization on training loss is robust to choice of learning rate. Fig. 11b shows that the improved training does not

lead to over-fitting. Reparameterized Adagrad achieves a marginally higher median validation accuracy at all learning rates. Reparameterized Adam achieves a marginally lower median maximum validation accuracy at learning rates between 4×10^{-3} and 0.02, but the difference amounts to less than half a percentage.

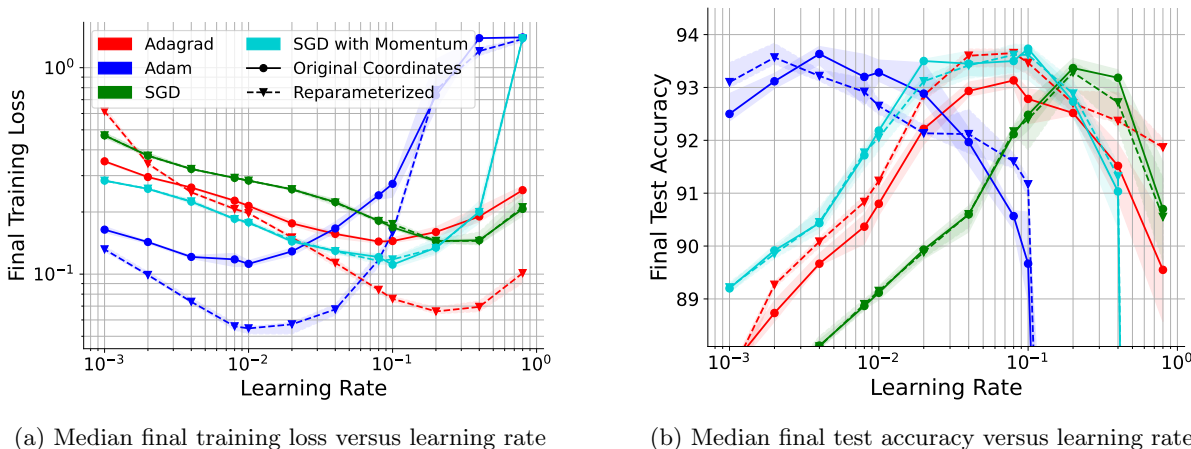


Figure 11: Training loss and test accuracy results for the fashionMNIST image classification task. Results are aggregated over independent trials corresponding to different random initializations. Medians are plotted as traces, and shaded regions indicate the 25th-75th percentiles.

We note that both Fig. 10b and Fig. 11b display small discrepancies between SGD in original coordinates and under reparameterization (and similarly for SGD with momentum), despite the fact that SGD is theoretically equivariant. We hypothesize that these discrepancies arise from the fact that matrix multiplication on GPUs is non-deterministic; because reparameterization involves additional matrix multiplications by the change-of-basis matrix V , this may lead to discrepancies arising from the nondeterministic accumulation of numerical error. We note that we do verify that our implementation yields identical results for SGD and SGD with momentum on CPU for small numbers of epochs.

Convex objectives Fig. 12 plots the gradient Euclidean norm over iterates for Adam, Adagrad, GD and GD with momentum. Unlike Fig. 5—where each algorithm uses the same learning rate in both original coordinates and under reparameterization, and this learning rate is tuned to produce the best performance in original coordinates—Fig. 12 shows results when learning rates are tuned separately in original coordinates versus under reparameterization. As a result, the discrepancy between Adagrad in original coordinates versus under reparameterization is more pronounced in Fig. 12a and Fig. 12c than in the corresponding plots in Fig. 5, while the qualitative results for logistic regression (Fig. 12b) are unchanged.

D Experimental details

Experiments were implemented in python, and both code and data will be made publicly available upon publication. Experiments with neural networks were implemented in Pytorch, and experiments with convex objectives were implemented using auto-differentiation in Jax and optimizers from Optax [27, 2, 10].

D.1 Dataset Details

UCI handwritten digits dataset The UCI digits dataset [1] contains 5620 instances, each an 8×8 pixel grayscale image of a handwritten digit of values $0, \dots, 9$. Each instance has a integer label, $0, \dots, 9$. We split the dataset into a training dataset with 3823 instances, a validation dataset with 598 instances, and a test dataset with 1199 instances.

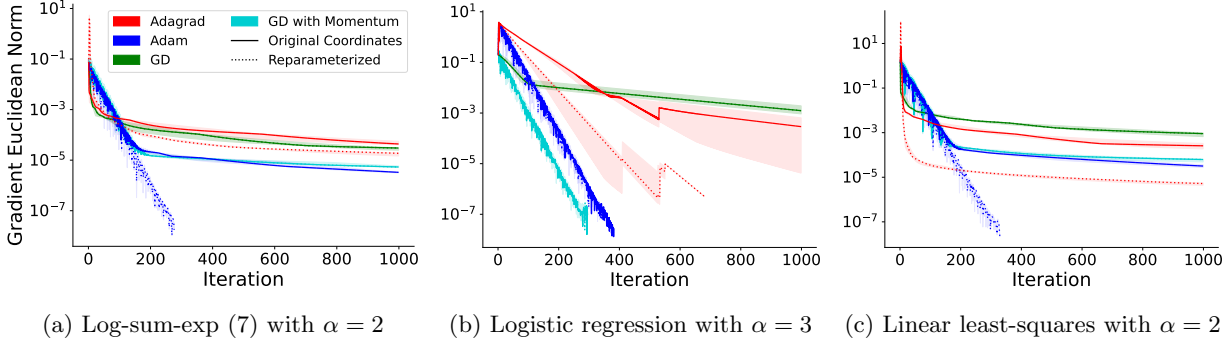


Figure 12: Counterpart to Fig. 5, where learning rates are tuned separately for methods in original coordinates versus under reparameterization. The discrepancy between Adagrad in original coordinates versus under reparameterization is more pronounced in Fig. 12a and Fig. 12c than in the corresponding plots in Fig. 5, while the qualitative results for logistic regression (Fig. 12b) are unchanged.

fashionMNIST dataset The fashionMNIST dataset consists of 28×28 pixel grayscale images of clothing, each having a label from one of 10 classes. For our experiments, we restrict to only instances corresponding to the first ten classes (labeled “t-shirt,” “trouser,” “pullover,” and “dress”). This yields a dataset of 28,000 instances, which we subdivide into a training set of 24,000 instances, a validation set of 1,000 instances, and a test set of 3,00 instances.

D.2 Algorithm Details

We consider four optimization algorithms: Adagrad, Adam, SGD, and SGD with momentum. We use standard settings for all hyperparameters except learning rate: for Adam, we use $\beta_1 = 0.9$ and $\beta_2 = 0.999$, and for SGD with momentum we use momentum parameter 0.9, matching that of Adam. We use zero weight decay for all algorithms, and for all objectives except the linear feed-forward networks, we use a constant learning rate schedule.

We tune learning rates for each algorithm. Unless otherwise noted, when choosing the range of learning rates to sweep for tuning, we use the following two-step procedure. First we sweep a coarse sweep using powers of 10 (e.g. $1e-3, 1e-2, \dots, 100$) to find an upper and lower bound on the learning rates that produce best performance. The metric by which we quantify the “best performance” for each different experiment is discussed below in Appendix D.5. We then perform a refined sweep, where we discretize each interval between subsequent power of 10 using doubling. For example, if the coarse sweep identified lower bound 0.01 and upper bound 1.0, we would perform the refined sweep over values $[0.01, 0.02, 0.04, 0.08, 0.1, 0.2, 0.4, 0.8, 1.0]$.

D.3 Details for Figures in Section 1

For Fig. 1 (left), we generate the loss landscape pictured by taking $d = 2$ dimensions and $n = 100$ samples. We generate a matrix A with singular values $\sigma_k = k^{-\alpha}$ with $\alpha = 1.5$ and random right- and left-singular vectors. We sampled $\theta^* \sim \mathcal{N}(0, \mathbb{I})$ and used A, θ^* to define the objective $f(\cdot)$ according to Eq. (7). We generated problem instances at random, and chose a random seed that produced a problem where the primary directions of variation for $f(\cdot)$ were clearly un-aligned with the coordinate axes. We allow Adagrad to take 1000 iterations.

We selected an initial point θ_0 that would produce a clear visual distinction between the two coordinate systems in early iterates. To select the learning rate, we first swept over the values $1, 10, 20, \dots, 100$, and examined the suboptimality of the solution produced after 1000 iterates. For each learning rate we conducted 5 random trials on log-sum-exp objectives generated with identical values of d, n, α , and with $\theta^* \sim \mathcal{N}(0, \mathbb{I})$; these trials were initialized at points drawn from $\mathbf{N}(0, \|\theta_0\|_2^2 \mathbb{I})$, where θ_0 is the initial point used in Fig. 1 (left). We found that for learning rates 30 through 90, the suboptimality of the solution returned by the algorithm in original coordinates was very comparable across learning rates and very close to zero ($< 1e-10$).

Thus we selected a learning rate with these properties that was on the lower end (hence 30) because at larger learning rates, the oscillations around the global minimum made it more difficult to visually assess the difference between trajectories before and after reparameterization.

D.4 Details for Figures in Section 4

Fig. 2 plots the eigenspectrum of an empirically estimated EGOP matrix. We consider a 2-layer ReLU network. Its first layer is a fully-connected linear layer with bias, with 64 input nodes and 32 output nodes, followed by a ReLU nonlinearity. Its second layer is a fully-connected linear layer with bias, with 32 input nodes and 10 output nodes, followed by a log-softmax. We form the function $f(\cdot)$ by taking the negative log-likelihood loss on the training dataset. We use the UCI digits dataset and consider the training subset described in Appendix D.1.

For Fig. 2 we use full-batch gradients to estimate the EGOP matrix. We take ρ to be a standard normal distribution: for each gradient sample, we form θ by sampling the entries of all weights and biases i.i.d. from a standard Gaussian. We estimate $\text{EGOP}(f)$ using $M = 10d$, where d is the total number of parameters (sum of all weight and bias entries) for the network. This is a larger number of EGOP samples than we use in later experiments; this is done intentionally with the goal of clearly resolving the spectral decay, rather than having decay appear as an artifact of numerical estimation with few samples.

For Fig. 6, we use the same dataset, architecture, objective $f(\cdot)$, and procedure for EGOP estimation, but we use different sampling distributions ρ . The “realistic initialization” distribution is described in full detail below in Appendix D.5.

For Fig. 7, we use the same architecture and objective for the UCI digits dataset. For fashionMNIST, we restrict to 4 classes and use the train-validation-test split, as described in D.1. Additionally, we down-sample the input to our network from 28×28 pixels to 14×14 pixels using a 2D max-pooling operation as the first layer of our network. The next layer is then a fully-connected linear layer with bias, with 196 input nodes and 20 output nodes, followed by a ReLU activation function. The last layer is a fully-connected linear layer with bias, with 20 input nodes and 4 output nodes. We form the function $f(\cdot)$ by taking the cross entropy loss on the training dataset. We note that this is equivalent to computing the log-softmax on the network output and then using negative log-likelihood loss, which is how we compute $f(\cdot)$ on tinyMNIST.

For Fig. 7, we use minibatches of size 300 to estimate gradients. For each architecture, we use $M = 5d$ gradient samples to estimate each block EGOP matrix, where d is the number of parameters in the network. This is a larger number of EGOP samples than we use in later experiments; this is done intentionally with the goal of clearly resolving the spectral decay, rather than having decay appear as an artifact of numerical estimation with few samples. We perform block EGOP reparameterization for both networks, where the blocks are defined by the weight matrices of each network. For more details on block reparameterization for neural network weights, see the example in Appendix B.

When drawing gradients to estimate the block EGOP matrices, the distribution over parameters ρ from which we draw is the same as a distribution we later use to initialize the networks during training. For a full description of this initialization distribution, see Appendix D.5.

D.5 Details for Figures in Section 6

Linear Feedforward Networks As described in Section 6, for Fig. 3 we consider parameters $\theta = [\text{vec}(W_1), \text{vec}(W_2), \text{vec}(W_3)]$ where $W_1 \in \mathbb{R}^{50 \times 10}$, $W_2 \in \mathbb{R}^{30 \times 50}$, $W_3 \in \mathbb{R}^{10 \times 30}$. We seek to minimize loss

$$f(\theta) = \|W_3 W_2 W_1 A - Y\|_F^2 / n_{\text{samples}}$$

where $A \in \mathbb{R}^{10 \times n_{\text{samples}}}$, and $Y = M^* A$ for $M^* \in \mathbb{R}^{10 \times 10}$ drawn from a standard Gaussian distribution. We induce spectral decay in $\text{EGOP}(f)$ by generating A with singular values $\sigma_k(A) = k^{-2}$ and random right- and left-singular vectors. For each trial, we generate 20,000 data samples, which we split into a test set of 10,000 training data instances, 4,000 validation instances, and 6,000 test instances. We define the training loss to be $f(\cdot)$ restricted to the training instances and their labels, and use this function when estimating the EGOP matrix. We use stochastic mini-batches of size 500 when estimating the EGOP and when performing optimization.

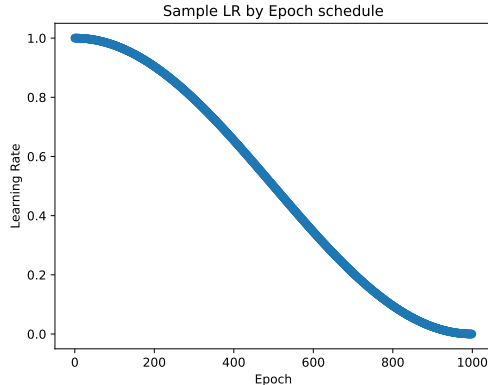


Figure 13: An example of the cosine annealing learning rate schedule used for the linear feedforward network experiments. This schedule corresponds to learning rate 1.0.

For each trial, we generate A, M^* , and Y as described above. We then estimate $\text{EGOP}(f)$ using $M = 2d$ samples, where d is the total number of parameters in the network ($d = 2,300$). When estimating the EGOP, we let ρ be the same distribution used when initializing networks for training. Specifically, we initialize each weight matrix from a mean-zero Xavier normal distribution, also called Glorot initialization, which is widespread in practice [13]. The Xavier normal distribution is a Gaussian with standard deviation $\sqrt{2/\text{fan-in-fan-out}}$, where for a matrix $W \in \mathbb{R}^{n \times m}$, $\text{fan-in-fan-out} = n + m$. We compute the full eigenvalue decomposition to find the change-of-basis matrix V .

We use 1000 epochs during training. See Appendix D.2 for choice of hyperparameters and choice of the range of learning rates to sweep for tuning. We measure performance using the median minimum validation loss achieved during training. We perform 10 independent trials at each learning rate. For each algorithm, we choose the learning rate at which the algorithm in original achieved lowest median minimum validation loss. Results of this learning rate sweep are in Fig. 3c.

Because Adam in original coordinates exhibited numerical instability due to the near-zero gradient values encountered, we used cosine annealing to decay the learning rate over the course of training. We use Pytorch’s default implementation of cosine annealing, and visualize an example of the learning rate schedule corresponding to learning rate 1.0 in Fig. 13. For ease of comparison, we apply the same learning rate decay schedule to all algorithms (Adagrad, Adam, SGD, and SGD with momentum) in both original and reparameterized coordinates. We use this learning rate decay schedule throughout learning rate tuning, and in all results displayed in Fig. 3.

ReLU Networks for Image Classification We use the UCI digits dataset and fashionMNIST, with the train-validation-split described in D.1. For the UCI digits dataset, we use a 2-layer ReLU network, with the same architecture and objective $f(\cdot)$ detailed in D.4. We use the same (random) partition of datapoints into train, validation, and test datasets for all trials.

For fashionMNIST, we restrict to 4 classes and use the train-validation-test split, as described in Appendix D.1. We use the architecture and objective $f(\cdot)$ described in Appendix D.4.

For both networks and objectives, we use minibatches of size 300 to estimate gradients throughout.

We perform block EGOP reparameterization for both networks, where the blocks are defined by the weight matrices of each network. For more details on block reparameterization for neural network weights, see the example in Appendix B. For each network, we use $M = d$ minibatch gradient samples to estimate the EGOP, where d is the number of parameters in the network.

For each objective and network, we use the same distribution over parameters for drawing gradient samples to estimate the EGOP and for initializing the network at training time. For the experiments in Fig. 4, that distribution is Pytorch’s default method for re-setting parameters in a linear layer, namely drawing weight entries i.i.d. from a uniform distribution with range $[-(\text{in-features})^{-1/2}, (\text{in-features})^{-1/2}]$ and drawing bias entries i.i.d. from a uniform distribution with range $[-(\text{fan-in-fan-out})^{-1/2}, (\text{fan-in-fan-out})^{-1/2}]$, where fan-in-fan-out for a layer is defined above in Appendix D.4. For the experiments in Fig. 1 (right),

we draw weight entries i.i.d. from a mean-zero Xavier distribution, and bias entries i.i.d. from a uniform distribution with range $[-(\text{fan-in-fan-out})^{-1/2}, (\text{fan-in-fan-out})^{-1/2}]$. All of these initialization distributions stem from heuristics that are widespread in practice, and the distinction between the weight distributions used with the digits dataset versus the fashionMNIST dataset was the result of using legacy code; we did not tune initializations to different applications.

See Appendix D.2 for choice of hyperparameters and choice of the range of learning rates to sweep for tuning. We used a constant learning rate for both datasets. We measure performance using the median maximum validation classification accuracy achieved during training. For each algorithm, we choose the learning rate at which the algorithm in original achieved highest median maximum validation accuracy. For the digits dataset, we performed 50 independent trials at each learning rate. For fashionMNIST, we performed 10 independent trials. We selected the number of epochs over which to train by examining loss and accuracy curves by eye, and choosing a value large enough that all algorithms had converged. For the digits dataset, we trained for 200 epochs, and for fashionMNIST we trained for 40 epochs.

Convex objectives We study three objectives. For each, we generate a matrix $A \in \mathbb{R}^{n_{\text{samples}} \times d}$ with singular value decay $\sigma_k = k^{-\alpha}$ and random orthonormal right- and left-singular vectors. The values of α are specified in the caption of Fig. 5. The log-sum-exp objective is defined in Eq. 5a. The logistic regression objective is defined as

$$f(\theta) = \sum_{i=1}^{n_{\text{samples}}} -y_i \log \left(\frac{1}{1 + e^{-\langle a_i, \theta \rangle}} \right) - (1 - y_i) \log \left(\frac{e^{-\langle a_i, \theta \rangle}}{1 + e^{-\langle a_i, \theta \rangle}} \right)$$

where $\{a_i \in \mathbb{R}^d\}_{i=1}^{n_{\text{samples}}}$ are the columns of A , and labels $y_i \sim \text{Bernoulli}(\pi(\theta^*)_i)$ where $\theta^* \in \mathbb{R}^d$ is drawn from $\mathcal{N}(0, \mathbb{I})$ and

$$\pi(\theta^*)_i \stackrel{\text{def}}{=} \frac{e^{-\langle a_i, \theta^* \rangle}}{1 + e^{-\langle a_i, \theta^* \rangle}}.$$

The logistic regression objective is

$$f(\theta) = \frac{1}{2} \|A\theta - y\|_2^2$$

where $y = A\theta^*$ and $\theta^* \in \mathbb{R}^d$ is drawn from $\mathcal{N}(0, \mathbb{I})$.

For log-sum-exp and linear least squares, $n_{\text{samples}} = d = 100$. For logistic regression, $n_{\text{samples}} = 100$ and $d = 3$.

For each objective, on each trial we generate A, θ^* , and thus $f(\cdot)$ randomly and independently following the above procedure.

For all convex objectives, use deterministic (full-batch) gradients to estimate the EGOP and to optimize.

For all objectives, we use $M = 5d$ gradient samples to estimate the EGOP matrix. We take ρ to be a standard Gaussian distribution, and use the same distribution to initialize when optimizing. See Appendix D.2 for choice of hyperparameters and choice of the range of learning rates to sweep for tuning. We used a constant learning rate for all convex objectives. We measure performance using the median final training loss achieved. For each algorithm, we choose the learning rate at which the algorithm in original achieved lowest median training loss. We perform 5 independent trials at each learning rate.

For each objective, we optimize for 1000 iterations, or until the gradient Euclidean norm drops below $1e - 8$. The latter termination condition is comparable to default termination conditions employed by `scipy.optimize` [33].

E Comparison with Other Reparameterization Methods

In this section, we compare the reparameterization method proposed in Algorithm 1 with SOAP and GaLore, two related methods that involve optimizing with Adam under change-of-basis [34, 40, 24]. To facilitate this discussion, we begin by instantiating an example of EGOP reparameterization for an objective whose parameters can be viewed as matrices, as this highlights some of the conceptual differences between the methods.

In many key applications of adaptive algorithms, including training neural networks, the parameters over which optimization occurs are matrix-valued. As a simple illustration, consider optimizing a single-layer linear fully-connected network. Let n_{in} denote the number of input features to the layer, and n_{out} denote the number of output features. This network then has $n_{\text{in}} \cdot n_{\text{out}}$ parameters, which can be expressed either as a vector, $\theta \in \mathbb{R}^{n_{\text{in}}n_{\text{out}}}$, or as a matrix, denoted $\text{mat}(\theta) \in \mathbb{R}^{n_{\text{in}} \times n_{\text{out}}}$.

Denote the training data and labels by $A \in \mathbb{R}^{n_{\text{in}} \times n_{\text{samples}}}$ and $Y \in \mathbb{R}^{n_{\text{out}} \times n_{\text{samples}}}$, and consider minimizing loss function

$$f(\theta) = \frac{1}{2} \|\text{mat}(\theta)^\top A - Y\|_F^2.$$

Similarly, the vector-valued gradients $\nabla f(\theta) \in \mathbb{R}^{n_{\text{in}}n_{\text{out}}}$ can also be viewed as matrices, $\text{mat}(\nabla f(\theta)) \in \mathbb{R}^{n_{\text{in}} \times n_{\text{out}}}$.

In the method proposed in this work, we consider gradients to be vector-valued when forming the EGOP. Thus for this single-layer objective, $\text{EGOP}(f) \in \mathbb{R}^{n_{\text{in}}n_{\text{out}} \times n_{\text{in}}n_{\text{out}}}$. We emphasize this vector-view of gradients for clarity, because the EGOP matrix has distinct eigenvectors from the expectation of the matrix product, $\text{mat}(\nabla f(\theta)) \text{mat}(\nabla f(\theta))^\top$. The related methods discussed in the introduction, including SOAP and GaLore, consider transformations by the matrices

$$\begin{aligned} Q_L &= \text{eigenvectors}(\mathbb{E}_{\theta \sim \rho}[\text{mat}(\nabla f(\theta)) \text{mat}(\nabla f(\theta))^\top]) \\ Q_R &= \text{eigenvectors}(\mathbb{E}_{\theta \sim \rho}[\text{mat}(\nabla f(\theta))^\top \text{mat}(\nabla f(\theta))]) \end{aligned}$$

and closely related transformations [34, 40, 24]. In general the eigenvectors in Q_L, Q_R correspond to different transformations than the eigenvectors of the EGOP. In particular, letting V denote the eigenbasis of the EGOP formed from vector-valued gradients, $V \neq Q_L \otimes Q_R$. Moreover, the class of orthonormal matrices obtainable from the EGOP eigenbasis is strictly more general than the class $Q_L \otimes Q_R$ for pairs of orthogonal matrices Q_L, Q_R , as formalized below:

Lemma 20. *For any orthogonal matrices $Q_L \in \mathbb{R}^{n_{\text{in}} \times n_{\text{in}}}, Q_R \in \mathbb{R}^{n_{\text{out}} \times n_{\text{out}}}$ and any objective function $f : \mathbb{R}^{n_{\text{in}}n_{\text{out}}} \rightarrow \mathbb{R}$, there exists orthogonal $V \in \mathbb{R}^{n_{\text{in}}n_{\text{out}} \times n_{\text{in}}n_{\text{out}}}$ such that*

$$\forall \theta \in \mathbb{R}^{n_{\text{in}}n_{\text{out}}}, \quad Q_L^\top \text{mat}(\nabla f(\theta))Q_R = \text{mat}(V\nabla f(\theta)).$$

However, there exist values of $n_{\text{in}}, n_{\text{out}}$, objective functions $f : \mathbb{R}^{n_{\text{in}}n_{\text{out}}} \rightarrow \mathbb{R}$, and orthogonal matrices $V \in \mathbb{R}^{n_{\text{in}}n_{\text{out}} \times n_{\text{in}}n_{\text{out}}}$ such that no orthogonal matrices $Q_L \in \mathbb{R}^{n_{\text{in}} \times n_{\text{in}}}, Q_R \in \mathbb{R}^{n_{\text{out}} \times n_{\text{out}}}$ satisfy

$$\forall \theta \in \mathbb{R}^{n_{\text{in}}n_{\text{out}}}, \quad Q_L^\top \text{mat}(\nabla f(\theta))Q_R = \text{mat}(V\nabla f(\theta)).$$

Proof. First we show that for any Q_L, Q_R , there exists suitable V satisfying the property. We begin by noting that for any matrices A, B, C of compatible dimension,

$$\text{vec}(ABC) = (C^\top \otimes A) \text{vec}(B).$$

Thus for any Q_L, Q_R ,

$$\text{vec}(Q_L^\top \text{mat}(\nabla f(\theta))Q_R) = (Q_R^\top \otimes Q_L^\top) \nabla f(\theta)$$

where the second equality uses the fact that trivially $\text{vec}(\text{mat}(\nabla f(\theta))) = \nabla f(\theta)$. The Kronecker product of orthogonal matrices is orthogonal, so choice of $V = (Q_R^\top \otimes Q_L^\top)$ satisfies the desired property.

We now show there exist orthogonal matrices $V \in \mathbb{R}^{n_{\text{in}}n_{\text{out}} \times n_{\text{in}}n_{\text{out}}}$ such that no orthogonal matrices $Q_L \in \mathbb{R}^{n_{\text{in}} \times n_{\text{in}}}, Q_R \in \mathbb{R}^{n_{\text{out}} \times n_{\text{out}}}$ satisfy

$$Q_R \otimes Q_L^\top = V.$$

This is a consequence of the fact that not all orthogonal matrices admit Kronecker product factorizations. Here we give one specific construction.

Let $\vec{1}_d$ denote the all-ones vector in \mathbb{R}^d . Consider V with leading column $v_1 = \vec{1}_{n_{\text{in}}n_{\text{out}}}/\sqrt{n_{\text{in}}n_{\text{out}}}$, and second column $v_2 = (n_{\text{in}}n_{\text{out}})^{-1/2} \cdot \text{concatenate}(\vec{1}_{n_{\text{in}}n_{\text{out}}/2}, -\vec{1}_{n_{\text{in}}n_{\text{out}}/2})$. Given the entries of v_1 are identical, this implies all the entries in the first column of Q_R are identical, and thus that the first n_{in} columns of V comprise concatenated copies of Q_L^\top . However this contradicts the fact that the entries of v_2 are identical in magnitude and nonzero but have positive sign for the first $n_{\text{in}}n_{\text{out}}/2$ entries and negative sign for the rest.

Thus no orthogonal matrices V with such first and second columns can be decomposed into $Q_R \otimes Q_L^T$, so in particular there exists some vector $z \in \mathbb{R}^{n_{\text{in}}n_{\text{out}}}$ such that

$$Q_R \otimes Q_L^T z \neq Vz.$$

Thus for any $f(\cdot)$ such that there exists θ with $\nabla f(\theta) = z$, it holds that for this value

$$Q_L^T \text{mat}(\nabla f(\theta)) Q_R = \text{mat}((Q_R \otimes Q_L^T) \nabla f(\theta)) \neq \text{mat}(V \nabla f(\theta)).$$

□

In both SOAP and GaLore the orthonormal bases are periodically re-computed, and performance of these methods degrades as time between re-computations grows [34, 40]. The fewest re-computations performed in the experiments of the original SOAP paper was once every 100 batches [34]. We show that with our proposed choice of basis, a single up-front computation of the change-of-basis suffices to improve the performance of both Adam and Adagrad in a variety of settings, as shown in Section 6. A valuable direction for future research would be to characterize the cost-benefit trade-off of periodic re-estimation of the change-of-basis matrix.

F Extended Discussion of Related Works

In this section, we expand on the overview of related work presented in Section 1.1.

Geometric sensitivity of adaptive methods A large body of research has been devoted to understanding the settings in which the per-coordinate learning rates of adaptive algorithms confer a benefit over more basic methods, such as (S)GD. Recently there has been renewed interest in distinguishing the properties of adaptive algorithms versus SGD because several empirical studies suggest that adaptive methods outperform SGD when training transformer models [20, 39]. Traditional analyses of Adagrad in the context of online convex optimization establish regret bounds which can be either better or worse than those enjoyed by SGD by up to a factor of \sqrt{d} , for d the number of problem parameters [12, 4]. More recent research has studied the rates at which adaptive methods converge to stationary points. Several works study convergence guarantees, measured in terms of the ℓ_2 norm of the gradient, on smooth non-convex objectives [35, 11]. These results show that Adagrad, Adam and related variants achieve rates matching those enjoyed by SGD, while having the key distinction that Adagrad and its variants do not require a-priori knowledge of the objective function’s Lipschitz constant [35, 11].

In order to shed light on the question of when adaptive algorithms enjoy provably stronger guarantees than SGD, a recent line of work studies convergence under more refined geometric assumptions, with particular emphasis on assumptions that are *not* rotationally invariant [18, 22, 37]. Xie et al. [37] establish convergence guarantees in terms of the L_∞ smoothness constant of the objective and also in terms of the related Hessian 1-norm. They show that rotationally invariant geometric assumptions do not suffice to capture settings when Adam out-performs SGD through experiments examining the sensitivity of Adam to orthonormal rotations [37].

Jiang et al. [18] and Liu et al. [22] study convergence of Adagrad on objectives that satisfy coordinate-wise smoothness. Both works prove similar convergence guarantees for Adagrad in terms of ℓ_1 gradient norm, rather than the ℓ_2 gradient norm measure more widely studied; Jiang et al. [18] establish convergence guarantees showing that SGD remains worst-case optimal even in the setting of coordinate-wise smoothness when measuring stationarity with the ℓ_2 gradient norm, motivating the need to measure stationarity with the ℓ_1 norm in order to prove separation between Adagrad and SGD. Using this ℓ_1 stationarity measure, Jiang et al. [18] establish provable separation between SGD’s and Adagrad’s convergence to stationary points of non-convex objectives. They show that when objective functions exhibit certain geometric properties, measured by their coordinate-wise smoothness constants, Adagrad’s upper bounds are lower than SGD’s lower bounds by a factor of d [18]. Our analysis builds on that of Jiang et al. [18] and Liu et al. [22], as a consequence of our results is that the EGOP reparameterization proposed in this work acts to transform objectives into the setting identified by Jiang et al. [18] where Adagrad’s convergence guarantees compare most favorably with SGD’s.

Ling et al. [21] develop a rotationally equivariant extension of Adam, termed VectorAdam, in an effort to reduce axis-aligned artifacts that arise when using adaptive methods to solve geometric optimization problems such as differentiable rendering. This method targets applications when the problem parameters $\theta \in \mathbb{R}^{r \cdot n}$ represent a collection of r different vectors in \mathbb{R}^n . VectorAdam uses the squared gradient norm of each n -dimensional vector to rescale the learning rates of all entries in each of the r vectors comprising θ , making the algorithm equivariant to transformations of the form $Q \text{mat } \theta$, where $\text{mat } \theta \in \mathbb{R}^{n \times r}$ is the reshaping of $\theta \in \mathbb{R}^{r \cdot n}$ and $Q \in \mathbb{R}^{n \times n}$ is orthonormal [21].

Change-of-basis for Optimization Several recent works propose that when using Adam and its variants to train neural networks, different choices of orthonormal transformation can reduce the computational cost associated with these algorithms and improve their performance [34, 24, 40]. In Section 1.1, we provided an overview of the work of Vyas et al. [34], Zhao et al. [40], and Maes et al. [24]. SOAP and GaLore both call for periodically re-computing the change-of-basis matrices. In their experiments, the fewest re-computations performed by Vyas et al. [34] was once every 100 batches, and they show that the performance gap between SOAP and Adam narrows as the number of batches between re-computations increases. In contrast, our we show that with our proposed choice of basis, a single up-front computation of the change-of-basis suffices to improve the performance of both Adam and Adagrad in a variety of settings, as shown in Section 6.

Outside of the domain neural network training, several works have considered data-driven methods for performing dimensionality reduction when optimizing objectives with low-rank EGOP matrices, including the works of Cartis et al. [3] and Cosson et al. [7]. For functions with low-dimensional active subspaces, Cartis et al. [3] study using the EGOP eigenbasis to reparameterize and reduce the dimension of optimization problems. They demonstrate that this approach yields computational speedups for loss functions whose EGOP matrix is low-rank. Cosson et al. [7] develop gradient descent algorithms which leverage the EGOP eigenbasis. Their method first estimates the EGOP and computes the corresponding leading r -eigenvectors, and then performs gradient descent steps along the directions of these r vectors. In the setting of exactly low-rank functions, they prove convergence results illustrating that this approach improves the dimensional dependency of gradient descent.